

Available online at [www.sciencedirect.com](http://www.sciencedirect.com)

SCIENCE @ DIRECT®

Tectonophysics xx (2005) xxx–xxx

TECTONOPHYSICS

[www.elsevier.com/locate/tecto](http://www.elsevier.com/locate/tecto)

# Thermochronology of allochthonous terranes in Ecuador: Unravelling the accretionary and post-accretionary history of the Northern Andes

R.A. Spikings<sup>a,\*</sup>, W. Winkler<sup>b</sup>, R.A. Hughes<sup>c</sup>, R. Handler<sup>d</sup><sup>a</sup>*Section des Sciences de la Terre, Université de Genève, Rue des Maraîchers 13, CH-1205 Genève 4, Switzerland*<sup>b</sup>*Geologisches Institut, ETH-Zentrum, Zürich CH-8092, Switzerland*<sup>c</sup>*British Geological Survey, Kingsley Dunham Center, Keyworth, Nottingham, NG12 5GG, United Kingdom*<sup>d</sup>*Institute for Geology and Palaeontology, University of Salzburg, Hellbrunner Str. 34/III, A-5020 Salzburg, Austria*

Received 25 November 2002; received in revised form 30 August 2003; accepted 23 December 2004

## Abstract

The western cordilleras of the Northern Andes (north of 5°S) are constructed from allochthonous terranes floored by oceanic crust. We present <sup>40</sup>Ar/<sup>39</sup>Ar and fission-track data from the Cordillera Occidental and Amotape Complex of Ecuador that probably constrain the time of terrane collision and post-accretionary tectonism in the western Andes. The data record cooling rates of 80–2 °C/my from temperatures of ~540 °C, during 85 to 60 Ma, in a highly tectonised mélange (Pujilí unit) at the continent–ocean suture and in the northern Amotape Complex. The rates were highest during 85–80 Ma and decelerated towards 60 Ma. Cooling was a consequence of exhumation of the continental margin, which probably occurred in response to the accretion of the presently juxtaposing Pallatanga Terrane. The northern Amotape Complex and the Pujilí unit may have formed part of a single, regional scale, tectonic mélange that started to develop at ~85 Ma, part of which currently comprises the basement of the Interandean Depression. Cooling and rotation in the allochthonous, continental, Amotape Complex and along parts of the continent–ocean suture during 43–29 Ma, record the second accretionary phase, during which the Macuchi Island Arc system collided with the Pallatanga Terrane. Distinct periods of regional scale cooling in the Cordillera Occidental at ~13 and ~9 Ma were synchronous with exhumation in the Cordillera Real and were probably driven by the collision of the Carnegie Ridge with the Ecuador Trench. Finally, late Miocene–Pliocene reactivation of the Chimbo–Toachi Shear Zone was coincident with the formation of the oldest basins in the Interandean Depression and probably formed part of a transcurrent or thrust system that was responsible for the inception and subsequent growth of the valley since ~6 Ma.

© 2005 Elsevier B.V. All rights reserved.

**Keywords:** Northern Andes; Terranes; Accretion; Thermochronology; Fission tracks; Ar isotopes

\* Corresponding author.

E-mail address: [spikings@terre.unige.ch](mailto:spikings@terre.unige.ch) (R.A. Spikings).

## 1. Introduction

The western Andean mountain ranges in Ecuador and Colombia, along the northwestern South American (SOAM) margin, are constructed from allochthonous terranes underlain by oceanic crust (Fig. 1). Debate currently exists regarding the accretionary history, specifically, the number of distinct terranes that exist, their origin and the timing of accretion against the northwestern SOAM margin. However, most workers broadly agree that the main accretionary phases in Ecuador occurred during the Middle–Late Cretaceous and Tertiary (Feininger and Bristow, 1980; McCourt et al., 1984; Feininger, 1987; Aspden and Litherland, 1992; Spikings et al., 2001; Hughes and Pilatasig, 2002).

Recent mapping of the Cordillera Occidental in Ecuador between 1°N and 4°S by the British Geological Survey (BGS-CODIGEM, 1997a,b, 1999, 2000) is the most extensive to date and identified two distinct terranes, which are separated by a regional scale, high strain shear zone and are juxtaposed against the Interandean Depression via a tectonic mélange (Figs. 1 and 2). Hughes and Pilatasig (2002) utilised regional structural and stratigraphic evidence and K/Ar ages from deformed granitoids to propose a model of terrane accretion, which envisaged accretionary phases during the Campanian and late Eocene. Spikings et al. (2001) proposed, on the basis of thermochronological evidence, that high rates of rock uplift and exhumation in the Cordillera Real during 65–55 Ma and 43–30 Ma were driven by increased compressive stress generated by terrane accretion to the west. However, no radiometric data have been obtained directly from the Cordillera Occidental that can be used to accurately constrain the timing of accretion.

Several workers have successfully used thermochronological methods to quantify the cooling, uplift and exhumation histories in autochthonous parts of the Andean orogen from Venezuela to Argentina (see review in Spikings et al., 2000). These studies provided a framework for the tectonic evolution of parts of the Andean chain that are composed of continental crust. We present new  $^{40}\text{Ar}/^{39}\text{Ar}$  and fission track data from both undeformed and highly strained, allochthonous rocks of the Cordillera Occidental of Ecuador, which define segments of the

thermal histories of the rocks between the temperatures of ~540 and 60 °C. The thermal histories permit a quantitative assessment of the timing, magnitude and duration of cooling and heating events and contribute to understanding the geological history of the northern Andes by constraining (i) the timing of accretion of terranes that comprise the Cordillera Occidental and, (ii) the post-accretionary tectonic history of the Ecuadorian Andes and their response to the subduction of heterogeneous oceanic crust.

## 2. Geological framework

Basement rocks north of 5°S can be divided into oceanic and continental domains (e.g., Lebrat et al., 1987). Within Ecuador, the continental domain is partly composed of a supra-crustal sequence of N–S striking, Palaeozoic–Lower Cretaceous metamorphic rocks of the Cordillera Real (Fig. 1), which together with Cretaceous and Tertiary sediments of the retro-arc Amazon Foreland Basin unconformably overlie the Precambrian Guyana Shield (Litherland et al., 1994). Upper Eocene–Pliocene volcanoclastic rocks in the Interandean Depression obscure the western limit of metamorphic rocks that form the Cordillera Real. However, negative Bouguer anomalies extend westward from the Cordillera Real across the Interandean Depression (Feininger and Seguin, 1983) and it is likely that metamorphic rocks form part of the basement within the Interandean Depression. This hypothesis is supported by the presence of metamorphic rocks on the eastern flank of the southern Cordillera Occidental (BGS-CODIGEM, 1997a) and the presence of metamorphic rocks within a tectonic mélange (Pujilí unit) on the western margin of the Interandean Depression (Fig. 2; Hughes and Pilatasig, 2002).

The allochthonous Amotape Complex, which is exposed in part in south-western Ecuador, is anomalous because the main structural trends are oriented east–west (Fig. 3). The complex can be divided into two sub-linear provinces: (i) a continental province, which mainly crops out to the south of the Naranjo Fault Zone and is comprised of the same rock units as those exposed in the Cordillera Real (Aspden et al., 1995; Noble et al., 1997) and (ii) a regional scale mélange zone (Palenque Mélange Division), which

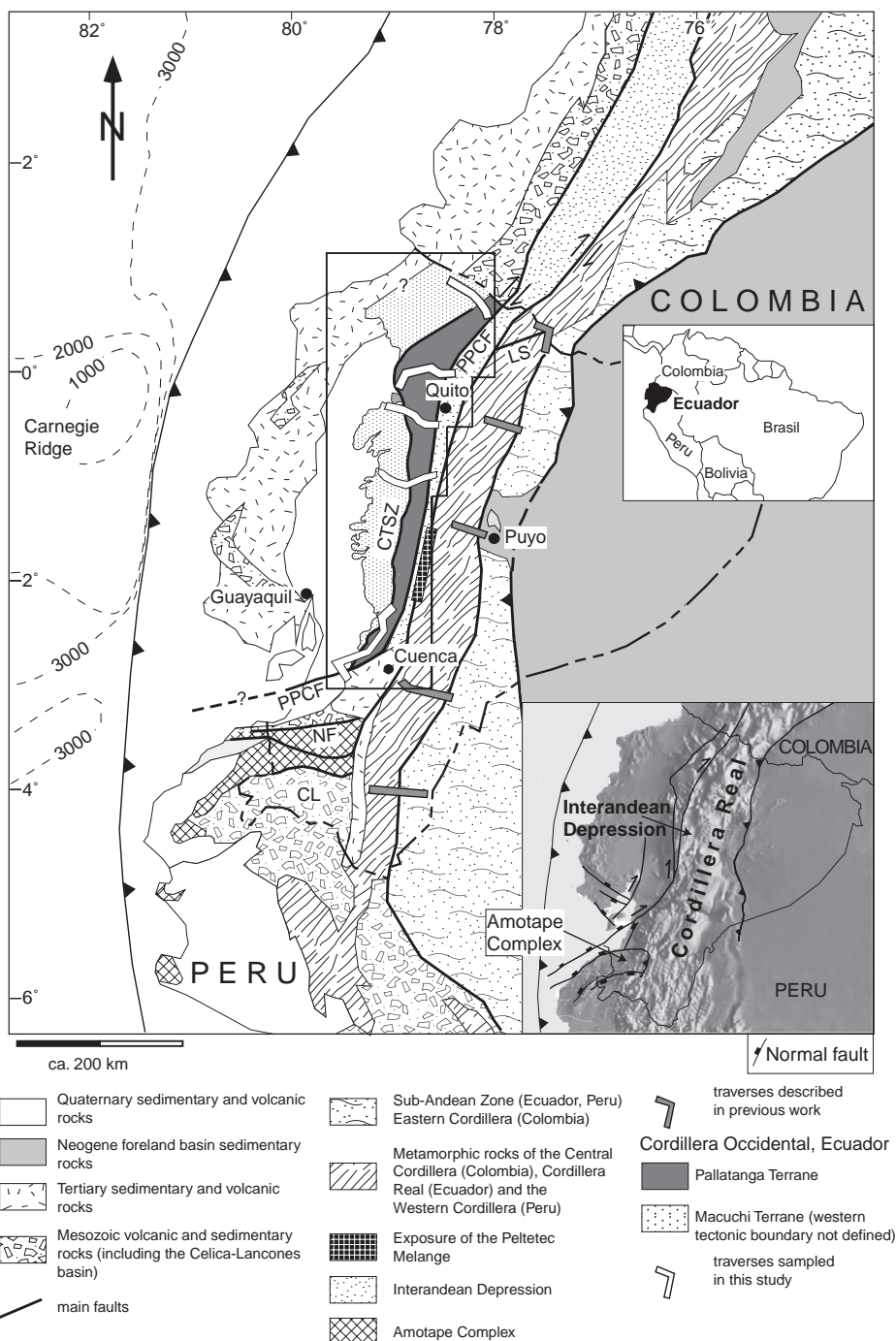


Fig. 1. Simplified geology of Ecuador showing the location of the Pallatanga Terrane, Macuchi Terrane and the Amotape Complex. Sampled traverses across the Cordillera Real (Spikings et al., 2000, 2001) and the Cordillera Occidental (this study) are shown. Black outline highlights the region of Fig. 2. Faults: PPCF: Pallatanga–Pujilí–Calacali fault, CTSZ: Chimbo–Toachi Shear Zone, LS: La Sofia fault, NF: Naranjo fault. Other abbreviations, CL: Celica–Lancones Basin.

**Legend****Quaternary - Pliocene**

- Volcanic and volcanoclastic rocks
- Some volcanic centers shown in italics

**Miocene**

- Chota Fm. (siliciclastic rocks)
- siliciclastic and volcanic rocks

**Early Miocene - Oligocene**

- Saraguro Group (volcanic rocks)

**Oligocene**

- Volcanic and siliciclastic rocks

- Silante Unit (siliciclastic and volcanic rocks)

**Eocene - Paleocene**

- siliclastic rocks, andesitic lavas
- Angamarca Group (siliclastic rocks, limestones)
- Cherts
- Macuchi Unit (volcanoclastic turbidites, hyaloclastites, pillow lavas, limestone)
- Saquisilí Unit (siliciclastic turbidites)

**Cretaceous****Maastrichtian - Campanian**

- Yunguilla Unit (and others) (siliclastic turbidites, basaltic lavas)
- siliclastic rocks, basaltic and andesitic lavas
- Mulaute Unit (volcanoclastic breccias, siliciclastic turbidites)
- Pilatón Unit (volcanoclastic turbidites)

**Campanian - older (?)**

- Pallatanga Unit (basalt, hyaloclastites, gabbro, peridotite, shale)
- San Juan Unit (anorthosite, gabbro, dolerite, peridotite)

**Jurassic**

- Undifferentiated metamorphic rocks

**Unassigned Ages**

- Intrusive rocks (granite, tonalite, gabbro, diorite)
- Pujilí Unit (tectonic melange, ultrabasic rocks, muscovite granites, amphibolites, pillow lavas)

**Faults**

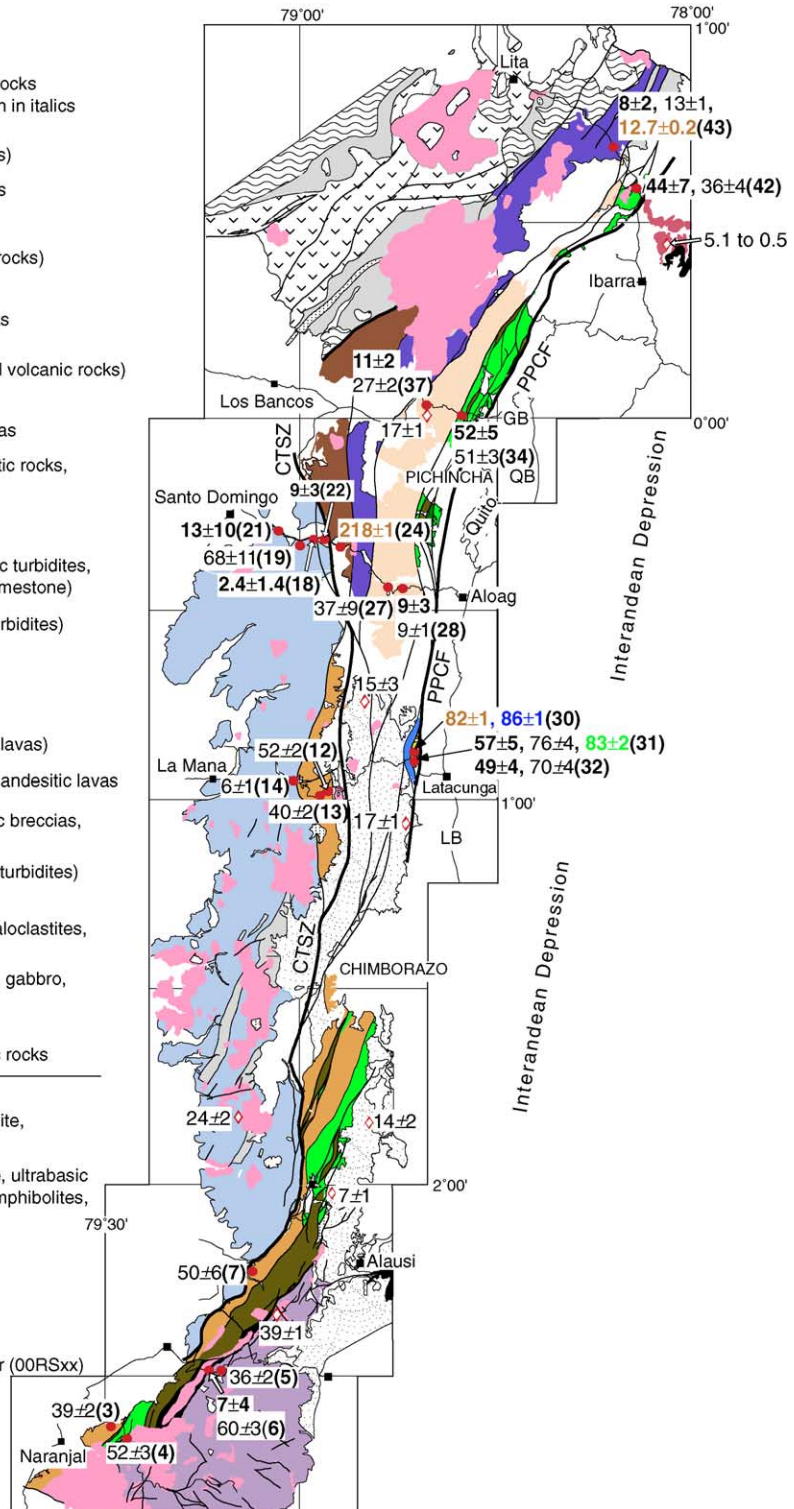
- Postulated terrane sutures
- Main faults

- Main road

- (7) Sample location and number (00RSxx)

- ◇ Previous work

- City





outcrops to the north of the Naranjo Fault Zone and encloses tectonic inclusions of high-pressure rocks (e.g., Arculus et al., 1999) of the Raspas unit. The northern province is interpreted to form part of an accretionary prism and non-mafic rocks of the southern province are considered to have been tectonically derived from the Cordillera Real at some time after 140 Ma (Aspden et al., 1995). The timing of decoupling of the complex from the Cordillera Real and its subsequent rotation within a dextral shear regime (e.g., Mourier et al., 1988; Mitouard et al., 1990) into the Andean forearc region is poorly constrained.

The oceanic domain of Ecuador underlies the Cordillera Occidental and consists of three distinguishable, allochthonous oceanic terranes (Fig. 1; e.g., Feininger and Bristow, 1980; Hughes and Pilatasig, 2002), which may have originated at the margins of the Caribbean Plateau (Spikings et al., 2001). The timing and accretion of these terranes are still a subject of debate, although Spikings et al. (2001) and Hughes and Pilatasig (2002) suggest the first collision occurred between the Pallatanga Terrane (Early–Late Cretaceous oceanic plateau basaltic and peridotitic basement) and the continental margin at some time between 80 and 60 Ma. The second stage of accretion involved the dextral collision of the oceanic, Paleocene (?)–early Eocene, volcanosedimentary arc sequence of the Macuchi Terrane with the Pallatanga Terrane, forming the Chimbo–Toachi Shear Zone at ~40 Ma (Figs. 1 and 2; Spikings et al., 2001; Hughes and Pilatasig, 2002). Pre-accretionary sedimentary sequences preserved in the Pallatanga Terrane include Santonian–Campanian turbidites (Wilkinson, 1998a), which are overlain by the Maastrichtian (Faucher et al., 1971; Wilkinson, 1998a) turbiditic Yunguilla unit that was partly sourced from metamorphic rocks of the Cordillera Real. The late Paleocene–Eocene turbiditic Angamarca group was deposited in a forearc setting subsequent to the accretion of the Pallatanga Terrane (Hughes and Pilatasig, 2002). Overlying sequences are dominated by late Eocene–early Oligocene (Wilkinson, 1998b) sedimentary rocks (Silante unit).

The boundary between the continental and oceanic provinces of the Cordillera Occidental and the metamorphic rocks underlying the Interandean Depression is defined by a tectonic mélange (Pujilí unit), which hosts, amongst others, meter scale blocks of metamorphic rocks that are also exposed in the Cordillera Real. This feature is regionally referred to as the Pallatanga–Pujilí–Calacali fault (Figs. 1 and 2). The western limit of the Macuchi Terrane is not exposed but may approximate to the distinct topographic break along the western flank of the Cordillera Occidental.

### 3. Recovery of thermal histories

The  $^{40}\text{Ar}/^{39}\text{Ar}$  method (e.g., McDougall and Harrison, 1999) has been used to determine single temperature–time points on a cooling path. The temperature range of each coordinate has been defined as the range in closure temperatures derived using Dodsonian theory (Dodson, 1973), assuming cooling rates between 100 and 10 °C/my. These temperature ranges are 545–511 °C, 390–350 °C and 360–325 °C for hornblende (spherical diffusion;  $\text{Do}/r^2=375$ ), white mica (plane sheet diffusion;  $\text{Do}/r^2=0.963$ ) and biotite (plane sheet diffusion;  $\text{Do}/r^2=342$ ), respectively (McDougall and Harrison, 1999). The time of each coordinate is determined after evaluation of the age spectrum (Fig. 4).

The temperature range at which fossil fission tracks within zircon and apatite partially anneal (partial annealing zone) is a complex function dominated by composition (Carlson et al., 1999) and thermal history. Unannealed track lengths in naturally derived apatite range between ~15.5 and 14.5  $\mu\text{m}$  (Gleadow et al., 1986) and hence samples that have mean track lengths in this range, combined with narrow track length distributions, experienced rapid cooling from temperatures greater than ~110 °C to temperatures lower than ~60 °C at the time indicated by the apatite fission track (AFT) age

Fig. 2. Geological map of the Cordillera Occidental, Ecuador, showing the locations of the main terrane sutures, the Interandean Depression and the Chota Basin (compiled from BGS-CODIGEM, 1997a,b, 1999, 2000). The locations of analysed samples and their fission-track ages are shown (hornblende  $^{40}\text{Ar}/^{39}\text{Ar}$ , green; white mica  $^{40}\text{Ar}/^{39}\text{Ar}$ , blue; hornblende  $^{40}\text{Ar}/^{39}\text{Ar}$ , brown; zircon fission track, bold italic; apatite fission track, bold). Fission track ages from previous studies, which were interpreted to record the stratigraphic age of the Saraguro group, Chota Basin and the intrusive age of various granitoids are also presented (Steinmann, 1997; Winkler et al., 2002). The values in brackets indicate the sample number (00RSxx series). See Fig. 1 for fault name abbreviations. GB: Guayllabamba Basin, LB: Latacunga Basin, QB: Quito Basin.

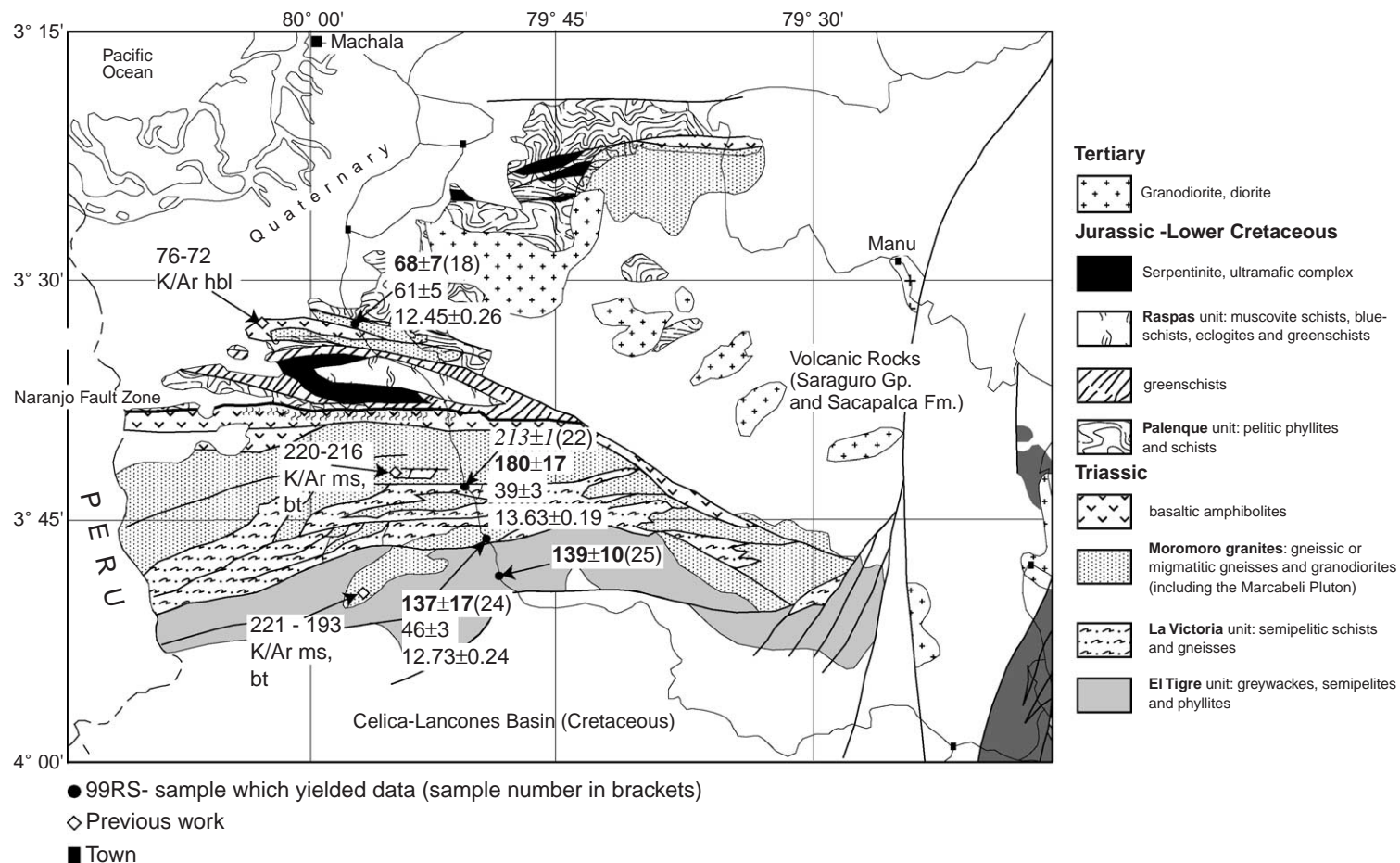


Fig. 3. Geological map of the Amotape Complex, Ecuador, modified from Aspdén et al. (1995). The locations of samples analysed in this study and their fission track ages are shown (biotite  $^{40}\text{Ar}/^{39}\text{Ar}$  plateau, italic; ZFT, bold; AFT, plain). K/Ar data from previous studies are also shown (hbl, hornblende; ms, muscovite; bt, biotite; Feininger and Silberman, 1982; Aspdén et al., 1992). The values in brackets indicate the sample number (99RSxx series).

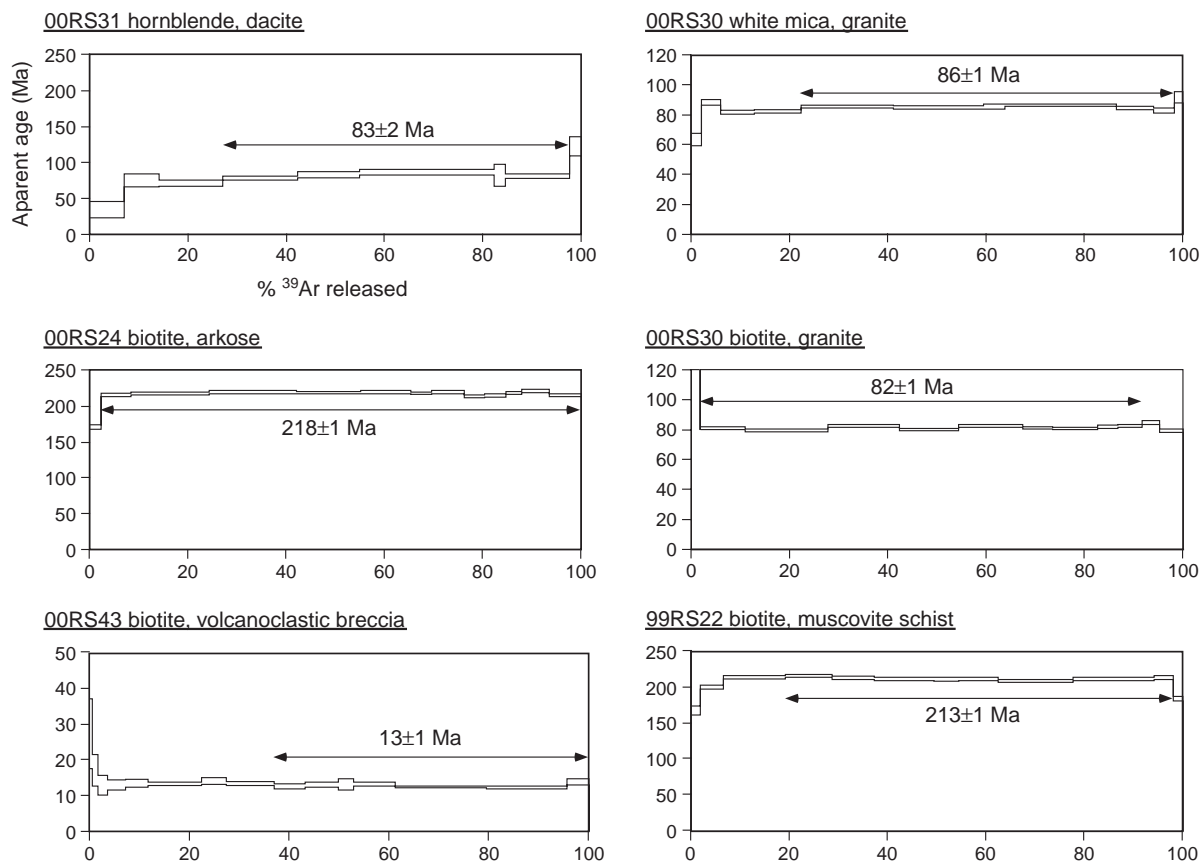


Fig. 4.  $^{40}\text{Ar}/^{39}\text{Ar}$  age spectra ( $\pm 1\sigma$ ) of various mineral phases from the Cordillera Occidental.

(Laslett et al., 1987). Broad track length distributions with shorter mean track lengths suggest a more complex thermal history, involving a significant amount of time within the partial annealing zone (Gleadow et al., 1986) relative to the AFT age. Thermal history solutions have been recovered from samples displaying mean track lengths  $<14.5\ \mu\text{m}$  following the approach described by Gallagher (1995) using the quantitative description of apatite annealing kinetics of Laslett et al. (1987). Apatite compositions have not been determined in this study. However, the magnitude of relative variation in temperature sensitivity for common apatite compositions (e.g.,  $<2\ \text{wt.}\%$  Cl and only minor substitution for  $\text{Ca}^{+2}$ ) is about  $\pm 30\ ^\circ\text{C}$  (Green et al., 1986). Therefore, while compositional variations may amplify or diminish the quantity of cooling and heating relative to standard (Durango) apatite, they

are considered relatively minor for the determination of the regional thermal history.

Similar principles apply to the interpretation of zircon fission track (ZFT) data although the lack of a suitable description of the annealing kinetics of tracks in zircon group minerals inhibits the reconstruction of potential thermal histories from track-length and age data. For the purpose of this study, the partial annealing zone is assumed to span between 300 and 220  $^\circ\text{C}$  (e.g., Tagami et al., 1998) and the mid-point of 260  $^\circ\text{C}$  has been plotted against the ZFT age to produce a single point on the thermal history path. When the single grain FT ages for an individual sample yield a  $p(\chi^2)$  value of  $<5\%$  it is assumed that more than one age population is present and individual age populations have been resolved (Galbraith and Green, 1990). Mineral separation and analytical procedures are provided in Appendix A.

## 4. Results

### 4.1. Cordillera Occidental

$^{40}\text{Ar}/^{39}\text{Ar}$ , ZFT and AFT ages were obtained from the Undifferentiated Metamorphics unit and both basement rocks and cover sequences of the Pallatanga and Macuchi Terranes along 5 traverses, which cross the Cordillera Occidental (Fig. 1). The age data are presented in Figs. 2 and 5 and Tables 1 and 2.

#### 4.1.1. Undifferentiated Metamorphics unit

Graphitic schists of the Undifferentiated Metamorphics unit (exposed south of 2°S) are considered to be separate to the Pallatanga Terrane (Fig. 2). The age of the rocks is unknown although they preserve similar fabrics and have identical lithologies to Jurassic schists exposed in the Cordillera Real (e.g., Litherland et al., 1994). Therefore, they probably formed part of the continental margin, which sutured against oceanic basement of the Pallatanga Terrane in the Late Cretaceous. ZFT and AFT ages of  $60 \pm 3$  and  $7 \pm 4$  Ma, yielded by a foliated schist (00RS6), are similar to ZFT and AFT ages yielded by similar Palaeozoic–Early Cretaceous lithologies exposed in the Cordillera Real (Spikings et al., 2001).

#### 4.1.2. Pallatanga Terrane

All data from the Pallatanga Terrane were obtained from blocks within the tectonic *mélange* (Pujilí unit; Fig. 2). The mafic and ultramafic basement rocks (Pallatanga unit) were barren of datable mineral phases.

**4.1.2.1. The tectonic *mélange* (Pujilí unit).** Samples 00RS30, 00RS31 and 00RS32 are from a locally exposed, chaotic and highly deformed tectonic *mélange* (Pujilí unit) that occupies a structural position along the eastern margin of the Cordillera Occidental between 0° and 1°S (Fig. 2; Hughes and Pilatasig, 2002). A coarse-grained, muscovite rich, granitic block, yields white mica and biotite  $^{40}\text{Ar}/^{39}\text{Ar}$  plateau ages of  $86 \pm 1$  and  $82 \pm 1$  Ma, respectively. A metamorphosed, foliated dacitic block from the *mélange*, which may have originally formed part of the Jurassic Undifferentiated Metamorphics unit (Fig. 2), yields a hornblende  $^{40}\text{Ar}/^{39}\text{Ar}$  plateau age of  $83 \pm 2$

Ma, a ZFT age of  $75 \pm 4$  Ma and an AFT age of  $57 \pm 5$  Ma with a partially annealed, mean track length of  $13.8 \pm 0.2$   $\mu\text{m}$ . A clast of early–middle Paleocene, turbiditic arkose (00RS32; Saquisilli unit) gives ZFT and AFT ages of  $70 \pm 4$  Ma and  $49 \pm 4$  Ma, respectively, and yields a partially annealed, mean AFT length of  $13.4 \pm 0.3$   $\mu\text{m}$ .

**4.1.2.2. The cover sequences.**  $^{40}\text{Ar}/^{39}\text{Ar}$ , ZFT and AFT ages from detrital grains of the sedimentary cover sequences of the Pallatanga Terrane have a complex distribution that includes pre-depositional ages, stratigraphic ages and post-depositional ages (Fig. 5). The variation in the relationship between the radiometric ages and the stratigraphic ages for any individual isotopic system is dependent on the structural position of the sample.

Several detrital populations from the Campanian Mulaute unit, Paleocene Saquisilli unit, late Paleocene–Eocene Angamarca group and the Oligocene Silante unit yield pre-depositional ZFT ages, which range between ~70 Ma and 320 Ma (Table 1). The Angamarca group, Silante unit and the volcanic, Oligocene–early Miocene, Saraguro group also yield ZFT ages from detrital and primary volcanic grains, which coincide with their stratigraphic ages and range between ~24 and ~60 Ma.

All ZFT and AFT ages from detrital grains of the Maastrichtian Yunguilla unit are younger than their stratigraphic age and range between ~36 and ~52 Ma (Fig. 5). Several sedimentary rocks of the Santonian Pilatón unit, Angamarca group and the Silante unit also yield ZFT and AFT ages that are younger than their stratigraphic ages and range between ~6 and ~24 Ma. A volcanic breccia in the Silante unit, located in central regions of the Pallatanga Terrane (00RS28) yields indistinguishable ZFT and AFT ages of  $9 \pm 3$  and  $9 \pm 1$  Ma. These ages are similar to the plateau biotite  $^{40}\text{Ar}/^{39}\text{Ar}$ , ZFT and AFT ages of  $12.7 \pm 0.2$  Ma,  $13 \pm 1$  and  $8 \pm 2$  Ma, respectively, that have been obtained from a volcanoclastic breccia of the Pilatón unit (00RS43) located in the northern Pallatanga Terrane (Fig. 1). The youngest detrital population is from an undeformed sandstone of the Angamarca group (00RS14) that is located very close (<1 km) to the Chimbo–Toachi Shear Zone (Fig. 2) and yields a ZFT age of  $6 \pm 1$  Ma.



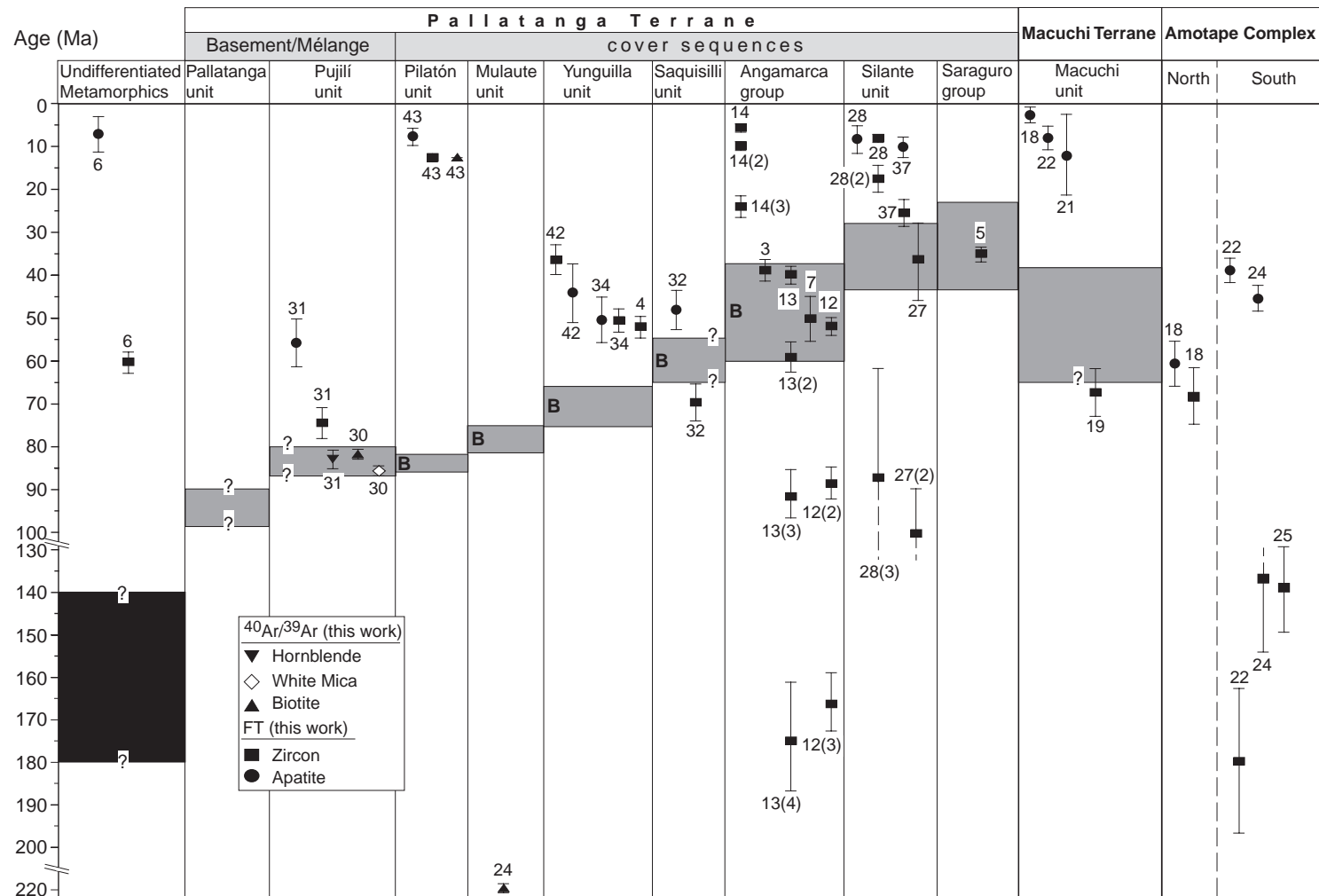


Fig. 5. Summary of  $^{40}\text{Ar}/^{39}\text{Ar}$ , ZFT and AFT data from the Cordillera Occidental and the Amotape Complex. Grey bands indicate the stratigraphic age of the rock sequence and a 'B' indicates that it was determined using fossil evidence; see text for references.

Table 1  
Fission-track ages from the Amotape Complex and the Cordillera Occidental of Ecuador

Sample number	Stratigraphy, lithology	Latitude	Longitude	Altitude (m)	No. of grains	Standard track density $\times 10^6$	Spontaneous track density $\times 10^6$	Induced track density $\times 10^6$	$p(\chi^2)$ (%)	U (ppm)	Fission track age $\pm 1\sigma$ (Ma)	Mean track length $\pm 1\sigma$ ( $\mu\text{m}$ )	Standard deviation ( $\mu\text{m}$ )
<i>Apatite</i>													
<i>Amotape Complex</i>													
99RS18	Limon Playa Unit, gneiss	S03 33 04	W79 56 56	sea level	24	1.143(5925)	0.3402(265)	1.226(955)	13	5	61.1 $\pm$ 5.1	12.45 $\pm$ 0.26(62)	2.01
99RS22	La Victoria Unit, Ms Bt schist	S03 42 11	W79 51 41	sea level	27	1.199(5925)	0.2477(409)	1.478(2441)	82	15	38.8 $\pm$ 2.7	13.63 $\pm$ 0.19(77)	1.68
99RS24	Marcabelli Pluton, granodiorite	S03 46 04	W79 49 27	685 $\pm$ ?	20	1.227(5925)	1.505(569)	7.817(2955)	31	80	45.6 $\pm$ 3.0	12.73 $\pm$ 0.24(84)	2.21
<i>Western Cordillera</i>													
<i>Undifferentiated Metamorphics unit</i>													
00RS6	Undiff Metamorphics, phylitic schist	S02 29 26.4	W79 14 06.1	1022 $\pm$ ?	3	1.462(6795)	0.0652(3)	2.500(115)	44	21	7.4 $\pm$ 4.3	N.D.	N.D.
<i>Pallatanga Terrane: tectonic melange</i>													
00RS31	Pujili Unit, dacite block	S00 51 04.8	W78 42 15.6	3015 $\pm$ ?	17	1.307(6795)	0.5410(176)	2.161(703)	13	21	56.5 $\pm$ 5.0	13.78 $\pm$ 0.24(70)	1.98
00RS32	Saquisilli Fm., arkosic arenite	S00 51 04.8	W78 42 15.6	3015 $\pm$ ?	17	1.359(6795)	0.7482(208)	4.032(1121)	95	37	48.6 $\pm$ 4.3	13.43 $\pm$ 0.28(44)	1.73
<i>Pallatanga Terrane: cover sequences</i>													
00RS28	Silante Unit, breccia	S00 26 23.0	W78 44 17.5	2058 $\pm$ 6	7	1.437(6795)	0.0372(7)	1.213(228)	80	11	8.5 $\pm$ 3.3	N.D.	N.D.
00RS34	Yungilla Unit, arkosic arenite	N00 00 22.8	W78 34 48.3	2362 $\pm$ 6	25	1.282(6795)	0.1283(145)	0.6150(695)	100	6	51.5 $\pm$ 5.3	N.D.	N.D.
00RS37	Silante Unit, volcanic tuff	N00 01 22.2	W78 39 13.1	1817 $\pm$ 5	28	1.385(6795)	0.0121(24)	0.2948(587)	99	3	10.9 $\pm$ 2.3	N.D.	N.D.
00RS42	Silante Unit?, lithic arenite	N00 36 03.6	W78 08 26.6	1390 $\pm$ 12	23	1.285(6925)	0.0941(45)	0.5356(256)	100	5	43.6 $\pm$ 7.3	N.D.	N.D.
00RS43	Pilaton Unit?, volcanoclastic breccia	N00 41 31.4	W78 12 05.0	1138 $\pm$ 5	32	1.510(6925)	0.0063(17)	0.2257(605)	100	2	8.2 $\pm$ 2.1	N.D.	N.D.
<i>Macuchi Terrane</i>													
00RS18	Macuchi Fm., basaltic andesite	S00 18 54.5	W78 57 20.2	805 $\pm$ 6	11	1.335(6925)	0.0046(3)	0.4977(324)	78	5	2.4 $\pm$ 1.4	N.D.	N.D.
00RS21	Macuchi Fm., volcanoclastic conglomerate	S00 17 01.6	W79 03 08.8	627 $\pm$ ?	17	1.260(6925)	0.0050(2)	0.0930(37)	100	1	13.2 $\pm$ 9.6	N.D.	N.D.
00RS22*	Macuchi Fm., basaltic andesite	S00 18 50.3	W78 55 53.7	866 $\pm$ 6	6	1.310(6925)	0.04049(10)	1.166(288)	40	11	8.8 $\pm$ 2.9	N.D.	N.D.
<i>Older Populations</i>													
00RS22	Macuchi Fm., basaltic andesite	S00 18 50.3	W78 55 53.7	866 $\pm$ 6	2	1.310(6925)	0.1667(13)	0.4744(37)	93	5	88.5 $\pm$ 28.8	N.D.	N.D.
<i>Zircon</i>													
<i>Amotape Complex</i>													
99RS18	Limon Playa Unit, gneiss	S03 33 04	W79 56 56	sea level	6	3.800 (2999)	11.68(406)	4.372 (152)	6	460	68 $\pm$ 6.8	N.D.	N.D.
99RS22	La Victoria Unit, Ms Bt schist	S03 42 11	W79 51 41	sea level	10	3.903 (2999)	13.86 (947)	1.991 (136)	23	204	180 $\pm$ 17	N.D.	N.D.
99RS24	Marcabelli Pluton, granodiorite	S03 46 04	W79 49 27	685 $\pm$ ?	6	4.006 (2999)	19.13 (420)	3.734 (82)	87	373	137 $\pm$ 17	N.D.	N.D.
99RS25*	El Tigre Unit, metagreywacke	S03 48 30	W79 48 43	890 $\pm$ ?	9	4.109 (2999)	20.80 (1307)	4.090 (257)	99	398	139 $\pm$ 10	N.D.	N.D.
<i>Older Populations</i>													
99RS25	El Tigre Unit, metagreywacke	S03 48 30	W79 48 43	890 $\pm$ ?	44	4.109 (2999)	19.76 (7690)	2.025 (788)	21	197	264 $\pm$ 13	N.D.	N.D.
<i>Western Cordillera</i>													
<i>Undifferentiated Metamorphics unit</i>													
00RS6	Undiff Metamorphics, graphitic schist	S02 29 26.4	W79 14 06.1	1022 $\pm$ ?	34	0.4571(3572)	9.319(3422)	4.746(1743)	12	415	60.1 $\pm$ 2.5	N.D.	N.D.

Pallatanga Terrane: tectonic melange													
00RS31	Pujili Unit, dacite block	S00 51 04.8	W78 42 15.6	3015±?	16	1.307(6795)	16.14(2501)	6.777(1050)	83	558	75.4±3.7	N.D.	N.D.
00RS32	Saquisilli Fm., arkosic arenite	S00 51 04.8	W78 42 15.6	3015±?	22	0.3509(3866)	10.33(1330)	3.457(445)	13	394	70.2±4.3	N.D.	N.D.
Pallatanga Terrane: cover sequences													
00RS3	Angamarca Gp., Ms arenite	S02 37 17.8	W79 27 42.4	382±7	20	0.3592(2078)	5.437(1184)	3.348(729)	24	364	39.0±2.3	N.D.	N.D.
00RS4*	Yungilla Unit, Ms arenite	S02 39 31.1	W79 26 47.2	856±7	26	0.4148(3572)	9.426(1794)	5.028(957)	37	473	52.1±2.6	N.D.	N.D.
00RS5	Saraguro Gp., Pl rich ignimbrite	S02 29 38.8	W79 13 06.1	1145±6	23	0.4359(3572)	6.728(1974)	5.538(1625)	21	508	35.5±1.6	N.D.	N.D.
00RS7	Angamarca Gp., Ms Hbl arenite	S02 12 08.1	W79 07 38.3	385±?	9	0.3936(3572)	10.43(477)		6	571	50.4±5.5	N.D.	N.D.
00RS12*	Angamarca Gp. Apagua Fm., sandstone	S00 57 42.9	W78 55 22.2	3957±5	16	0.4994(3572)	11.78(2609)	7.583(1679)	6	607	52.0±2.2	N.D.	N.D.
00RS13*	Angamarca Gp. Apagua Fm., sandstone	S00 58 52.6	W78 56 24.5	3881±9	8	0.3706(2078)	8.034(1083)	4.985(672)	75	538	40.1±2.3	N.D.	N.D.
00RS14*	Angamarca Gp. Apagua Fm., sandstone	S00 56 48.6	W79 00 14.4	2417±5	4	0.4049(2078)	1.282(79)	6.265(386)	71	619	5.6±0.7	N.D.	N.D.
00RS27*	Silante Unit, lithic arenite	S00 26 29.8	W78 46 29.8	1610±5	2	0.4506(2078)	3.825(35)	3.196(29)	41	281	36.5±9.2	N.D.	N.D.
00RS28*	Silante Unit, breccia	S00 26 23.0	W78 44 17.5	2058±6	12	0.4620(2078)	1.074(205)	3.818(729)	38	322	8.7±0.7	N.D.	N.D.
00RS34	Yungilla Unit, arkosic arenite	N00 00 22.8	W78 34 48.3	2362±6	26	0.3652(3866)	4.022(1590)	1.923(760)	98	211	51.2±2.7	N.D.	N.D.
00RS37	Silante Unit, volcanic tuff	N00 01 22.2	W78 39 13.1	1817±5	33	0.3866(3866)	1.622(662)	1.568(640)	100	158	26.9±1.7	N.D.	N.D.
00RS42	Yungilla Unit, lithic arenite	N00 36 03.6	W78 08 26.6	1390±12	7	4.009(3866)	3.018(232)	2.251(173)	11	225	36.1±3.8	N.D.	N.D.
00RS43	Pilaton Unit, volcanoclastic breccia	N00 41 31.4	W78 12 05.0	1138±5	9	4.080(3866)	4.423(518)	9.255(1084)	83	885	13.1±0.8	N.D.	N.D.
Older populations													
00RS4	Yungilla Unit, Ms arenite	S02 39 31.1	W79 26 47.2	856±7	17	0.4148(3572)	16.98(1761)	4.233(439)	15	408	111.0±6.7	N.D.	N.D.
00RS12	Angamarca Gp., arkose	S00 57 42.9	W78 55 22.2	3957±5	20	0.4994(3572)	12.57(4093)	4.722(1538)	45	378	88.8±3.7	N.D.	N.D.
00RS12	Angamarca Gp., arkose	S00 57 42.9	W78 55 22.2	3957±5	5	0.4994(3572)	12.11(1012)	2.417(202)	90	194	166.2±13.7	N.D.	N.D.
00RS13	Angamarca Gp. Apagua Fm., sandstone	S00 58 52.6	W78 56 24.5	3881±9	11	0.3706(2078)	8.158(1060)	3.425(445)	87	370	59.1±3.8	N.D.	N.D.
00RS13	Angamarca Gp. Apagua Fm., sandstone	S00 58 52.6	W78 56 24.5	3881±9	11	0.3706(2078)	9.773(1401)	2.630(377)	83	284	92.0±6.1	N.D.	N.D.
00RS13	Angamarca Gp. Apagua Fm., sandstone	S00 58 52.6	W78 56 24.5	3881±9	11	0.3706(2078)	12.41(1787)	1.744(251)	97	188	175.2±13.1	N.D.	N.D.
00RS13	Angamarca Gp. Apagua Fm., andstone	S00 58 52.6	W78 56 24.5	3881±9	17	0.3706(2078)	16.81(2841)	1.272(215)	95	137	321.7±24.5	N.D.	N.D.
00RS14	Angamarca Gp. Apagua Fm., sandstone	S00 56 48.6	W79 00 14.4	2417±5	18	0.4049(2078)	2.396(475)	6.028(1195)	79	581	10.8±0.7	N.D.	N.D.
00RS14	Angamarca Gp. Apagua Fm., sandstone	S00 56 48.6	W79 00 14.4	2417±5	2	0.4049(2078)	7.700(155)	8.644(174)	53	854	24.2±2.8	N.D.	N.D.
00RS27	Silante Unit, lithic arenite	S00 26 29.8	W78 46 29.8	1610±5	8	0.4506(2078)	10.16(434)	3.044(130)	25	264	100.5±10.5	N.D.	N.D.
00RS28	Silante Unit, breccia	S00 26 23.0	W78 44 17.5	2058±6	7	0.4620(2078)	2.290(197)	3.976(342)	91	336	17.9±1.7	N.D.	N.D.
00RS28	Silante Unit, breccia	S00 26 23.0	W78 44 17.5	2058±6	1	0.4620(2078)	6.855(51)	2.419(18)	100	210	87.5±24.1	N.D.	N.D.
Macuchi Terrane													
00RS19	Macuchi Fm., basaltic andesite	S00 19 09.8	W78 59 20.1	766±?	5	0.4163(2078)	16.20(415)	6.167(158)	1	578	67.5±10.7	N.D.	N.D.

Numbers in parentheses are the number of tracks counted, no track lengths and hence standard deviations in track lengths have been measured in the zircon crystals.

When  $p(\chi^2)$  is <5% the fission track age is the central age, otherwise it is the pooled age. Sample codes in bold type indicate those samples which yielded both apatite and zircon FT ages.

All zircon and apatite separates were counted by R. Spikings. See Appendix A for analytical details.

Bt, biotite; Hbl, hornblende; Ms, Muscovite; N.D., No data; Pl, Plagioclase.

\* Denotes sample which is comprised of >1 source population. The age of the older population is listed under 'populations'.

Table 2

 $^{40}\text{Ar}/^{39}\text{Ar}$  ages from the Amotape Complex and the Cordillera Occidental

Step	$^{36}\text{Ar}/^{39}\text{Ar}$	$^{37}\text{Ar}/^{39}\text{Ar}$	$^{40}\text{Ar}^*/^{39}\text{Ar}_K$	$^{40}\text{Ar}^*$ (%)	Cumulative $^{39}\text{Ar}(\%)$	Age Ma $\pm 1\sigma$
Cordillera Occidental						
<i>Hornblende</i>						
00RS31, $J=0.01680\pm0.00017$ , dacite, S00° 51' 04.8", W78° 42' 15.6"						
1	0.225315 $\pm$ 0.001209	1.624637 $\pm$ 0.000766	67641600 $\pm$ 0.385640	1.6	7.0	35.2 $\pm$ 11.5
2	0.090345 $\pm$ 0.001009	4.420118 $\pm$ 0.001195	28919377 $\pm$ 0.303057	7.7	7.0	75.8 $\pm$ 8.8
3	0.029624 $\pm$ 0.000451	15.041618 $\pm$ 0.001353	10015927 $\pm$ 0.133607	12.6	13.0	72.1 $\pm$ 4.0
4	0.018044 $\pm$ 0.000356	19.924283 $\pm$ 0.001166	6444921 $\pm$ 0.105458	17.3	15.2	79.0 $\pm$ 3.2
5	0.013884 $\pm$ 0.000487	20.286637 $\pm$ 0.001485	5335503 $\pm$ 0.144097	23.1	12.8	83.4 $\pm$ 4.2
6	0.011329 $\pm$ 0.000429	21.934545 $\pm$ 0.001570	4559058 $\pm$ 0.126859	26.6	13.1	86.5 $\pm$ 3.8
7	0.016987 $\pm$ 0.000459	23.609272 $\pm$ 0.001720	6111469 $\pm$ 0.136001	17.9	14.2	86.9 $\pm$ 4.0
8	0.015659 $\pm$ 0.001760	25.192637 $\pm$ 0.007348	5453950 $\pm$ 0.520966	15.2	2.2	82.8 $\pm$ 15.1
9	0.013470 $\pm$ 0.000379	24.613175 $\pm$ 0.001573	4802017 $\pm$ 0.112165	17.1	13.0	81.3 $\pm$ 3.3
10	0.011044 $\pm$ 0.001589	24.964496 $\pm$ 0.006353	5502669 $\pm$ 0.470136	40.7	2.5	123.4 $\pm$ 13.4
Plateau: steps 4–9					70.5	82.9 $\pm$ 1.6
<i>White Mica</i>						
00RS30, $J=0.01675\pm0.00017$ , coarse granite, S00° 51' 04.8", W78° 42' 15.6"						
1	0.033932 $\pm$ 0.000508	1.225717 $\pm$ 0.000350	12.090043 $\pm$ 0.150571	17.1	2.1	63.6 $\pm$ 4.4
2	0.011104 $\pm$ 0.000212	6.080808 $\pm$ 0.000284	5.816811 $\pm$ 0.062897	43.6	3.8	88.4 $\pm$ 2.0
3	0.003394 $\pm$ 0.000111	1.308549 $\pm$ 0.000106	3.689956 $\pm$ 0.032878	72.8	6.9	82.0 $\pm$ 1.2
4	0.002077 $\pm$ 0.000078	1.513178 $\pm$ 0.000087	3.311092 $\pm$ 0.023145	81.5	9.4	82.7 $\pm$ 1.0
5	0.002212 $\pm$ 0.000049	1.652601 $\pm$ 0.000053	3.449813 $\pm$ 0.014509	81.1	18.9	85.9 $\pm$ 0.9
6	0.002286 $\pm$ 0.000055	1.354070 $\pm$ 0.000058	3.469257 $\pm$ 0.016429	80.5	18.4	85.1 $\pm$ 1.0
7	0.002526 $\pm$ 0.000185	2.266910 $\pm$ 0.000181	3.492108 $\pm$ 0.054732	78.6	4.3	85.8 $\pm$ 1.8
8	0.000808 $\pm$ 0.000035	2.633043 $\pm$ 0.000045	2.977581 $\pm$ 0.010507	92.0	22.7	86.5 $\pm$ 0.9
9	0.000805 $\pm$ 0.000082	0.680713 $\pm$ 0.000123	3.076196 $\pm$ 0.024153	92.3	7.6	84.9 $\pm$ 1.1
10	0.001499 $\pm$ 0.000163	1.412324 $\pm$ 0.000210	3.168052 $\pm$ 0.048204	86.0	4.2	83.3 $\pm$ 1.6
11	0.000762 $\pm$ 0.000400	0.956997 $\pm$ 0.000432	3.284005 $\pm$ 0.118351	93.1	1.7	91.9 $\pm$ 3.5
Plateau: steps 5–11					77.7	85.6 $\pm$ 0.4
<i>Biotite</i>						
00RS24, $J=0.01673\pm0.00017$ , arkose, S00° 19' 56.1", W78° 52' 15.0"						
1	0.046018 $\pm$ 0.000334	0.491110 $\pm$ 0.000167	19514100 $\pm$ 0.099656	30.3	2.3	170.9 $\pm$ 3.2
2	0.009025 $\pm$ 0.000088	0.055671 $\pm$ 0.000052	10275380 $\pm$ 0.026302	74.0	6.1	215.9 $\pm$ 2.2
3	0.002478 $\pm$ 0.000029	0.053780 $\pm$ 0.000020	8409333 $\pm$ 0.008666	91.3	15.8	217.7 $\pm$ 2.1
4	0.000557 $\pm$ 0.000018	0.026664 $\pm$ 0.000021	7924237 $\pm$ 0.005519	97.9	17.8	219.8 $\pm$ 2.1
5	0.000393 $\pm$ 0.000024	0.036407 $\pm$ 0.000027	7853220 $\pm$ 0.007527	98.5	13.1	219.3 $\pm$ 2.1
6	0.000456 $\pm$ 0.000032	0.081359 $\pm$ 0.000031	7876990 $\pm$ 0.009517	98.3	10.2	219.5 $\pm$ 2.1
7	0.000401 $\pm$ 0.000074	0.231407 $\pm$ 0.000080	7806035 $\pm$ 0.022306	98.5	4.2	218.4 $\pm$ 2.1
8	0.000352 $\pm$ 0.000048	0.081458 $\pm$ 0.000053	7845436 $\pm$ 0.014239	98.7	6.6	219.5 $\pm$ 2.1
9	0.000573 $\pm$ 0.000056	0.252742 $\pm$ 0.000074	7688514 $\pm$ 0.017019	97.8	4.1	213.9 $\pm$ 2.1
10	0.000719 $\pm$ 0.000073	0.256922 $\pm$ 0.000069	7769023 $\pm$ 0.021840	97.3	4.3	214.9 $\pm$ 2.1
11	0.000554 $\pm$ 0.000095	0.334970 $\pm$ 0.000090	7850011 $\pm$ 0.028442	97.9	3.3	218.6 $\pm$ 2.2
12	0.000592 $\pm$ 0.000047	0.303099 $\pm$ 0.000048	7959328 $\pm$ 0.014165	97.8	5.5	221.1 $\pm$ 2.1
13	0.000535 $\pm$ 0.000045	0.337675 $\pm$ 0.000046	7732678 $\pm$ 0.013371	98.0	6.6	215.6 $\pm$ 2.1
Plateau: steps 2–13					97.7	217.8 $\pm$ 0.6
00RS30, $J=0.01678\pm0.00017$ , coarse granite, S00° 51' 04.8", W78° 42' 15.6"						
1	0.754541 $\pm$ 0.000842	0.143848 $\pm$ 0.000164	238.811955 $\pm$ 0.301526	6.6	1.9	425.3 $\pm$ 8.1
2	0.030115 $\pm$ 0.000083	0.059497 $\pm$ 0.000027	11.663828 $\pm$ 0.024585	23.7	9.0	81.5 $\pm$ 1.1
3	0.015205 $\pm$ 0.000037	0.071119 $\pm$ 0.000017	7.207233 $\pm$ 0.010878	37.7	16.8	80.1 $\pm$ 0.8
4	0.008830 $\pm$ 0.000030	0.822105 $\pm$ 0.000031	5.363977 $\pm$ 0.008865	51.4	14.6	82.9 $\pm$ 0.9
5	0.005629 $\pm$ 0.000038	0.254884 $\pm$ 0.000026	4.371833 $\pm$ 0.011343	62.0	12.1	80.3 $\pm$ 0.9



Table 2 (continued)

Step	$^{36}\text{Ar}/^{39}\text{Ar}$	$^{37}\text{Ar}/^{39}\text{Ar}$	$^{40}\text{Ar}^*/^{39}\text{Ar}_K$	$^{40}\text{Ar}^*$ (%)	Cumulative $^{39}\text{Ar}(\%)$	Age Ma $\pm 1\sigma$
Cordillera Occidental						
<i>Biotite</i>						
00RS30, $J=0.01678\pm0.00017$ , coarse granite, S00° 51' 04.8", W78° 42' 15.6"						
6	0.003771 $\pm$ 0.000028	0.139245 $\pm$ 0.000026	3.911990 $\pm$ 0.008349	71.5	13.0	82.6 $\pm$ 0.8
7	0.003207 $\pm$ 0.000028	0.102962 $\pm$ 0.000048	3.714624 $\pm$ 0.017235	74.5	6.1	81.7 $\pm$ 0.9
8	0.003132 $\pm$ 0.000045	0.114092 $\pm$ 0.000035	3.672550 $\pm$ 0.013470	74.8	9.0	81.1 $\pm$ 0.9
9	0.001867 $\pm$ 0.000098	0.108415 $\pm$ 0.000080	3.336203 $\pm$ 0.028936	83.5	4.2	82.2 $\pm$ 1.2
10	0.002461 $\pm$ 0.000075	0.159198 $\pm$ 0.000059	3.530193 $\pm$ 0.022054	79.4	4.8	82.8 $\pm$ 1.0
11	0.001331 $\pm$ 0.000092	0.133793 $\pm$ 0.000087	3.271737 $\pm$ 0.027295	88.0	3.7	85.0 $\pm$ 1.1
12	0.001953 $\pm$ 0.000082	0.198592 $\pm$ 0.000067	3.269654 $\pm$ 0.024125	82.4	4.7	79.7 $\pm$ 1.0
Plateau: steps 2–10					89.7	81.6 $\pm$ 0.3
00RS43, $J=0.01682\pm0.00017$ , volcanoclastic breccia, N00° 41' 31.4", W78° 12' 05.0"						
1	0.041766 $\pm$ 0.001105	1202271 $\pm$ 0.000947	13173369 $\pm$ 0.328405	6.3	0.5	27.4 $\pm$ 9.8
2	0.011158 $\pm$ 0.000491	1524799 $\pm$ 0.000479	3759634 $\pm$ 0.145135	12.3	1.2	17.1 $\pm$ 4.4
3	0.004186 $\pm$ 0.000308	0.351471 $\pm$ 0.000289	1651235 $\pm$ 0.091101	25.1	1.9	12.9 $\pm$ 2.7
4	0.002333 $\pm$ 0.000164	0.081418 $\pm$ 0.000151	1128582 $\pm$ 0.048504	38.9	3.6	13.0 $\pm$ 1.5
5	0.001025 $\pm$ 0.000126	0.013359 $\pm$ 0.000112	0.764335 $\pm$ 0.037320	60.4	4.5	13.5 $\pm$ 1.1
6	0.000636 $\pm$ 0.000047	0.031097 $\pm$ 0.000052	0.641385 $\pm$ 0.013992	70.7	10.8	13.3 $\pm$ 0.4
7	0.000424 $\pm$ 0.000091	0.057254 $\pm$ 0.000101	0.601485 $\pm$ 0.027018	79.2	5.0	14.1 $\pm$ 0.8
8	0.000382 $\pm$ 0.000055	0.035419 $\pm$ 0.000062	0.568203 $\pm$ 0.016396	80.1	9.5	13.4 $\pm$ 0.5
9	0.000207 $\pm$ 0.000078	0.068291 $\pm$ 0.000084	0.489587 $\pm$ 0.022969	87.5	6.3	12.6 $\pm$ 0.7
10	0.000155 $\pm$ 0.000074	0.078856 $\pm$ 0.000084	0.487958 $\pm$ 0.021899	90.6	6.6	13.1 $\pm$ 0.7
11	0.000174 $\pm$ 0.000177	0.138493 $\pm$ 0.000197	0.490869 $\pm$ 0.052218	89.5	3.0	13.1 $\pm$ 1.6
12	0.000088 $\pm$ 0.000055	0.065305 $\pm$ 0.000066	0.472342 $\pm$ 0.016143	94.5	8.4	13.2 $\pm$ 0.5
13	0.000061 $\pm$ 0.000025	0.046495 $\pm$ 0.000030	0.438115 $\pm$ 0.007395	95.9	18.3	12.3 $\pm$ 0.3
14	0.000107 $\pm$ 0.000035	0.161805 $\pm$ 0.000044	0.443258 $\pm$ 0.010314	92.9	16.2	12.4 $\pm$ 0.3
15	0.000184 $\pm$ 0.000103	0.215827 $\pm$ 0.000124	0.513744 $\pm$ 0.030448	89.4	4.3	13.9 $\pm$ 0.9
Plateau: steps 8–15					72.5	12.7 $\pm$ 0.2
Amotape Complex						
<i>Biotite</i>						
99RS22, $J=0.01657\pm0.00017$ , muscovite schist, S03° 42' 11", W79° 51' 41"						
1	0.072587 $\pm$ 0.000723	0.097592 $\pm$ 0.000460	27385564 $\pm$ 0.218328	21.7	1.8	169.1 $\pm$ 6.2
2	0.010329 $\pm$ 0.000234	0.034845 $\pm$ 0.000185	10184186 $\pm$ 0.069432	70.0	4.8	201.2 $\pm$ 2.7
3	0.002684 $\pm$ 0.000079	0.045703 $\pm$ 0.000065	8460222 $\pm$ 0.023520	90.6	12.5	215.5 $\pm$ 2.1
4	0.001647 $\pm$ 0.000118	0.024090 $\pm$ 0.000095	8205537 $\pm$ 0.034877	94.1	9.5	216.8 $\pm$ 2.2
5	0.001275 $\pm$ 0.000113	0.023261 $\pm$ 0.000099	8014301 $\pm$ 0.033558	95.3	8.6	214.6 $\pm$ 2.2
6	0.001746 $\pm$ 0.000079	0.057472 $\pm$ 0.000060	8070402 $\pm$ 0.023402	93.6	12.3	212.5 $\pm$ 2.1
7	0.001092 $\pm$ 0.000196	0.185473 $\pm$ 0.000174	7849898 $\pm$ 0.058378	95.9	5.0	212.0 $\pm$ 2.5
8	0.000619 $\pm$ 0.000123	0.092757 $\pm$ 0.000108	7727309 $\pm$ 0.036605	97.6	8.0	212.3 $\pm$ 2.2
9	0.000525 $\pm$ 0.000059	0.036518 $\pm$ 0.000057	7609971 $\pm$ 0.017526	98.0	15.2	209.8 $\pm$ 2.0
10	0.000608 $\pm$ 0.000091	0.024521 $\pm$ 0.000079	7733686 $\pm$ 0.027038	97.7	10.4	212.4 $\pm$ 2.1
11	0.000850 $\pm$ 0.000101	0.026871 $\pm$ 0.000113	7816213 $\pm$ 0.030583	96.8	6.0	212.7 $\pm$ 2.2
12	0.000848 $\pm$ 0.000179	0.029521 $\pm$ 0.000214	7901074 $\pm$ 0.053547	96.8	3.9	215.0 $\pm$ 2.5
13	0.001770 $\pm$ 0.000298	0.057005 $\pm$ 0.000355	7051698 $\pm$ 0.089632	92.6	1.9	185.0 $\pm$ 3.0
Plateau: steps 4–12					80.5	213.0 $\pm$ 0.7

Corrected for post-irradiation decay of  $^{37}\text{Ar}$  ( $T_{0.5}=35.1$  days) and  $^{39}\text{Ar}$  ( $T_{0.5}=269$  years).

See Appendix A for analytical and data processing details.

#### 4.1.3. Macuchi Terrane

ZFT and AFT ages from the northern, Paleocene (?)–Eocene Macuchi unit show a large scatter from ~2

to ~68 Ma (Figs. 2 and 5). The oldest age of  $68\pm11$  Ma (undeformed basaltic andesite; 00RS19) may approximate the maximum stratigraphic age of the

unit, which is not clearly defined. The remaining ages are younger than their stratigraphic ages. Basaltic andesite (00RS18) from a 1 m wide, mylonitic shear band along the Chimbo–Toachi Shear Zone yields a significantly younger AFT age of  $2.4 \pm 1.4$  Ma, which is the youngest AFT age obtained from the Cordillera Occidental. The shear band forms part of an extensive high strain zone, which contains S–C mylonite fabrics that consistently indicate dextral movement (Hughes and Pilatasig, 2002). Undeformed basaltic andesite (00RS22) adjacent to the Chimbo–Toachi Shear Zone yields an AFT age of  $9 \pm 3$  Ma. Further west, an undeformed volcanoclastic conglomerate of the same unit (00RS21) yields an imprecise AFT age of  $13 \pm 10$  Ma. The low precision is a consequence of the extremely low uranium concentration in the sample (1 ppm).

#### 4.2. Amotape Complex

A N–S traverse, oriented approximately normal to the structural strike, was sampled through the Amotape Complex (Fig. 3).

##### 4.2.1. North of the Naranjo Fault Zone

Indistinguishable ZFT and AFT ages of  $68 \pm 6.8$  Ma and  $61 \pm 5$  Ma and an intermediate mean AFT length of  $12.45 \pm 0.26$   $\mu\text{m}$  have been obtained from Late Triassic gneisses (99RS18) of the Moromoro Granitoid Complex, located to the north of the Naranjo Fault Zone (Table 1).

##### 4.2.2. South of the Naranjo Fault Zone

South of the Naranjo Fault Zone, Paleozoic schists (99RS22) yield a biotite  $^{40}\text{Ar}/^{39}\text{Ar}$  plateau age of  $213 \pm 1$  Ma and a ZFT age of  $180 \pm 17$  Ma, which is significantly older than the ZFT age from the north. A weakly metamorphosed, Early Paleozoic metagreywacke (99RS25) and a Late Triassic pluton (Marcabelli Pluton; 99RS24), yield similar ZFT ages of  $139 \pm 10$

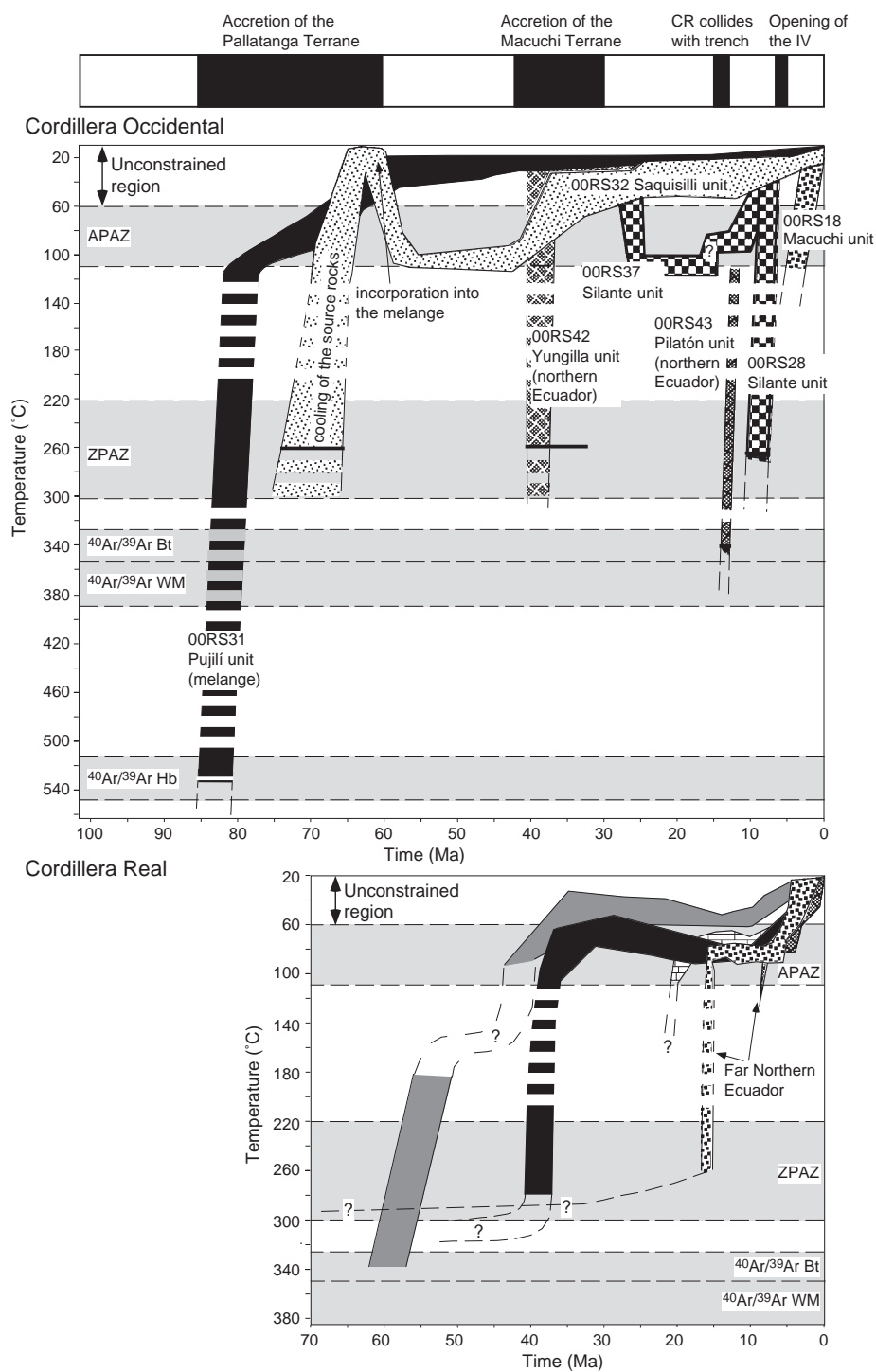
and  $137 \pm 17$  Ma, respectively. The Marcabelli Pluton yields a U/Pb (zircon) age of  $228 \pm 1$  Ma and biotite K/Ar ages ranging between 221 and 193 Ma (Aspden et al., 1992; Noble et al., 1997), which are older than the ZFT ages reported here. The metagreywacke also yields an older ZFT population with an age of  $264 \pm 13$  Ma. The Marcabelli Pluton and Paleozoic schists yield similar AFT ages of  $46 \pm 3$  Ma (99RS24) and  $39 \pm 3$  Ma (99RS22) and mean AFT lengths of  $12.73 \pm 0.24$  and  $13.63 \pm 0.19$   $\mu\text{m}$ , respectively.

## 5. Interpretation

### 5.1. Thermal history of the Cordillera Occidental

AFT ages from the Cordillera Occidental range between 88 and 2 Ma although a majority of the apatites have low uranium abundances ( $<10$  ppm) and hence only two samples yielded track-length data. Therefore, it is not possible to directly determine potential thermal histories for all of the samples from the fission-track data by forward modelling. Rather, potential thermal history envelopes have been constructed (Fig. 6) by interpolating between the apatite partial annealing zone, zircon partial annealing zone and Ar retention zones when either (i) the  $^{40}\text{Ar}/^{39}\text{Ar}$  and FT ages are indistinguishable or (ii) the earliest rapid cooling event identified in the AFT thermal history model is indistinguishable from either the  $^{40}\text{Ar}/^{39}\text{Ar}$  and/or the ZFT age. The Laslett et al. (1987) model was calibrated with an initial induced track length of 16.3  $\mu\text{m}$  although we use an initial track length of 15.5  $\mu\text{m}$  because (i) it has been shown that the annealing model underestimates track annealing at low temperatures (Vrolijk et al., 1992), which results in exaggerating cooling rates at temperatures below about 60 °C, and (ii) all published, fossil track lengths in apatite standards are less than or equal to 15.5  $\mu\text{m}$  (e.g., Gleadow et al., 1986).

Fig. 6. Thermal history envelopes for samples from the Cordillera Occidental (this study; derived assuming an unannealed track length of 15.5  $\mu\text{m}$ ), representative thermal history envelopes from metamorphic rocks of the Cordillera Real (Spikings et al., 2001) and their relationship to significant tectonic events in Ecuador. The thermal history envelopes are 95% confidence envelopes within the region of the APAZ and their widths through the ZPAZ and Ar retention zones are mainly coincident with the ZFT or  $^{40}\text{Ar}/^{39}\text{Ar}$  age ( $\pm 1\sigma$ ), respectively (shown by the horizontal red line). Dashed envelopes highlight those areas that are interpolated. The  $^{40}\text{Ar}/^{39}\text{Ar}$  white mica (WM) and biotite (Bt) zones of isotopic closure are defined by the variation in closure temperature between cooling rates of 50 and 10 °C/APAZ: apatite partial annealing zone, CR: Carnegie Ridge, IV: Interandean Depression, ZPAZ: zircon partial annealing zone.



### 5.1.1. Undifferentiated Metamorphics unit

The lack of track length data and the low precision AFT age from the Undifferentiated Metamorphics unit render it invalid to reconstruct the thermal histories of the metamorphic rocks exposed in the Cordillera Occidental. However, the ages are identical to those found in the Cordillera Real and it is possible that they have a similar general history as those exposed in the Cordillera Real (Fig. 6; Spikings et al., 2001). Therefore, rapid cooling of the southern Cordillera Occidental during 65–55 Ma and since 9 Ma, as experienced by the Cordillera Real (e.g., >30 °C/my; Spikings et al., 2000), could account for the fission-track ages in the Undifferentiated Metamorphics unit.

### 5.1.2. Pallatanga Terrane: tectonic mélange

Modelled temperature–time paths (Fig. 6) for a foliated dacitic block (00RS31) from the tectonic mélange (Pujilí unit), reveal cooling from 110–80 °C to as low as 20 °C during ~80–60 Ma at moderate rates (~2–3 °C/my). However, interpolation between the modelled path into the temperature zone of  $^{40}\text{Ar}$  loss in hornblende at  $83 \pm 2$  Ma, suggests that cooling rates were much greater (~80 °C/my) during ~85–80 Ma. Similar white mica and biotite  $^{40}\text{Ar}/^{39}\text{Ar}$  ages from a granitic block (00RS30) in the same mélange also record cooling between 85 and 80 Ma. Cooling of the mélange blocks during 85–60 Ma overlaps with that identified in the Cordillera Real (65–55 Ma; Fig. 1; Spikings et al., 2001), which was attributed to exhumation driven by the collision of the Pallatanga Terrane with the continental margin and probably dates the formation and subsequent exhumation of the mélange. Modelled thermal history envelopes of a sandstone block of the Saquisillí Fm. (00RS32), which force the paths to reach surface temperatures during 65–60 Ma (stratigraphic age of the sample), prefer a thermal path that shows heating to ~110 °C during 64–55 Ma (Fig. 6), followed by an increased cooling rate to temperatures <60 °C during ~42–32 Ma. The ZFT age of the sample ( $70 \pm 4$  Ma) is similar to its stratigraphic age, which implies that the source region was cooling at high rates (say >60 °C/my through a static geothermal gradient of 30 °C/km) during ~74–64 Ma from temperatures of ~260 °C.

### 5.1.3. Pallatanga Terrane: cover sequences

Detrital grains from the pre-accretionary, Santonian Pilatón unit in northern Ecuador (00RS43) record post-depositional heating (burial?) and subsequent cooling of the rocks. The indistinguishable biotite  $^{40}\text{Ar}/^{39}\text{Ar}$  and ZFT ages record a period of rapid cooling at ~13 Ma (Fig. 6) from >340 to <260 °C. The younger AFT age precludes interpolating the T–t path between 260 and 110 °C although the AFT age is indistinguishable from AFT cooling ages derived from the northernmost Cordillera Real (Fig. 1; Spikings et al., 2001) and may have experienced a similar cooling history involving an increase in cooling rate at ~9 Ma (Fig. 6).

Indistinguishable ZFT and AFT ages of detrital grains from the Maastrichtian Yunguilla unit in northern Ecuador (00RS42) record rapid cooling from temperatures >260 °C to <60 °C at ~40 Ma (Fig. 6), implying that the sedimentary rock must have been heated to temperatures in excess of 260 °C, which was probably caused by both tectonic and sedimentary burial. Further south, indistinguishable ZFT and AFT ages from detrital grains of the same unit (Fig. 1) may record rapid cooling from temperatures >260 °C at ~50 Ma. However, the sample (00RS34) has experienced hydrothermal alteration and it is possible that the FT ages relate to mineral growth and cooling following hydrothermal heating.

The late Paleocene–Eocene Angamarca group was partly derived from metamorphic rocks of the Cordillera Real (Hughes and Pilatasig, 2002), parts of which were exhuming at rates of 1.6 km/my during 43–30 Ma (Spikings et al., 2000). Therefore, those sedimentary rocks with ZFT ages of ~40 Ma may have been derived from fault blocks within the Cordillera Real that were exhuming at similarly high rates, exposing very young ZFT ages at the surface and their present day ZFT ages approximate their residence times within the Angamarca group. The older (pre-depositional) ages were derived from a source region that did not exhume rapidly at 40 Ma and preserve an older source history.

The ZFT age of the youngest detrital population in the Angamarca group (00RS14;  $6 \pm 1$  Ma), which is located proximal to the Chimbo–Toachi Shear Zone (Fig. 2), is a result of an increase in cooling rate during the late Miocene as a consequence of either exhumation driven by reactivation of the fault or reheating via hydrothermal fluids, which have infil-



trated the fault. The sample must have been heated to temperatures  $>260^{\circ}\text{C}$  prior to the late Miocene.

A stratigraphic ZFT age from tuffaceous sandstone within the post accretionary, upper Eocene–Oligocene Silante unit in northern Ecuador (00RS37) records the time of eruption of the andesitic source rocks (Fig. 5). However, the younger AFT age of  $11 \pm 2$  Ma records post-depositional heating to temperatures  $>60^{\circ}\text{C}$  and subsequent cooling. The age may be a mixed age caused by increased cooling rates at 15 and 9 Ma, similar to that which occurred in the northern Cordillera Real (Fig. 6; Spikings et al., 2001). Post-depositional and indistinguishable ZFT and AFT ages of  $\sim 9$  Ma obtained from a breccia of the Silante unit (00RS28; Fig. 1) suggest that the sample was heated and subsequently rapidly cooled from temperatures  $>260^{\circ}\text{C}$  to  $<60^{\circ}\text{C}$  at  $\sim 9$  Ma (Fig. 6). Heating of the sample may have been caused by burial beneath the volcanic Silante Group and younger rocks derived from the Cordillera Real. Alternatively, these rocks may have been overthrust by the Cordillera Real at  $\sim 15$  Ma (Spikings et al., 2001).

The volcanic Saraguro Group is a post-accretionary volcanic sequence that was deposited within southern Ecuador. The ZFT age yielded by an ignimbrite of the Saraguro Group in southern Ecuador (00RS5;  $36 \pm 2$  Ma) is similar to a series of ZFT ages ranging between 42 and 25 Ma from older units of the Saraguro Group (Steinmann, 1997; Hungerbühler et al., 2002) and probably records the time of eruption (Fig. 5).

#### 5.1.4. Macuchi Terrane

Hughes and Pilatasig (2002) compiled K/Ar and radiolarian data from the Macuchi unit and showed that it is older than late Eocene and may be as old as the Paleocene. Therefore, the imprecise ZFT age of  $68 \pm 11$  Ma (00RS19) from undeformed basaltic andesite of the Macuchi unit may simply record cooling following eruption and confirms that the Macuchi unit contains Paleocene sequences. The similarity between the ZFT and stratigraphic age indicates that they have remained cooler than  $\sim 60^{\circ}\text{C}$  since the Paleocene, and hence this sample has not been buried to depths greater than  $\sim 6.5$  km since its eruption (assuming a geothermal gradient of  $30^{\circ}\text{C}/\text{km}$ ; Henry, 1981).

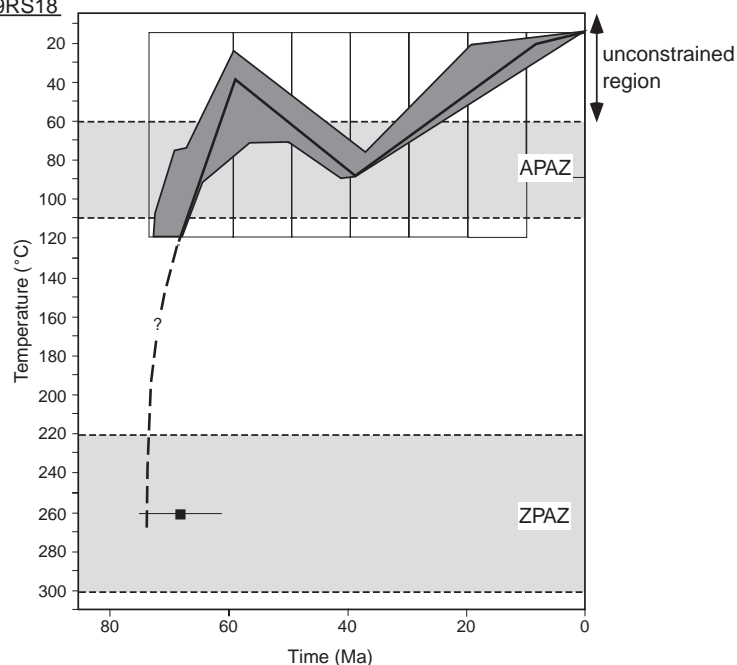
The Miocene and younger AFT ages from the Macuchi unit (Fig. 5) reflect post eruption heating (to

temperatures  $>60^{\circ}\text{C}$ ) and subsequent cooling episodes. The late Pliocene AFT age of sheared basaltic andesite (00RS18) probably relates to latest Miocene–Pliocene or more recent cooling caused by exhumation and possibly brittle reactivation of the Chimbo–Toachi Shear Zone (Fig. 6). The AFT age of sample 00RS22 ( $9 \pm 3$  Ma; Fig. 2), located in western exposures of the Macuchi unit cannot be used to constrain its thermal history. However, it is likely that this sample may have cooled through the apatite partial annealing zone at  $\sim 9$  Ma, similar to what has been recorded in parts of the Pallatanga Terrane and the Cordillera Real (Spikings et al., 2001).

#### 5.2. Thermal history of the Amotape Complex

Mean AFT lengths from the Amotape Complex are partially annealed and therefore the AFT ages in these samples do not correspond to specific cooling ‘events’. Modelled thermal histories for all samples from the Amotape Complex show that they experienced  $\leq 90$ – $40^{\circ}\text{C}$  of heating during 60–39 Ma (Fig. 7). There is no evidence of an increased geothermal gradient (e.g., volcanism) within the Amotape Complex during this period. Therefore, it is likely that heating was a consequence of burial beneath Paleocene volcanic rocks (e.g., Hungerbühler et al., 2002; Jaillard et al., 1999; Fig. 8) and Eocene sequences such as the Angamarca group and the lower Saraguro group that are no longer preserved in the region. An additional characteristic that is common to all samples is the onset of cooling at  $\sim 43$ – $39$  Ma (Fig. 7). The samples cooled at rates of  $\sim 5.5$ – $4.5^{\circ}\text{C}/\text{my}$  (south of the Naranjo Fault Zone) and  $\sim 5.0$ – $4.0^{\circ}\text{C}/\text{my}$  (north of the Naranjo Fault Zone) at some time during 43–29 Ma and the cooling rate gradually decreased after 30 Ma south of the Naranjo Fault Zone. Sample 99RS18, located north of the Naranjo Fault Zone, cooled from  $90$ – $75^{\circ}\text{C}$  to the present day surface ( $15^{\circ}\text{C}$ ) after 41 Ma although samples located to the south of the Naranjo Fault Zone cooled from  $120$  to  $95^{\circ}\text{C}$  (Fig. 7). Cooling through an assumed static geothermal gradient of  $30^{\circ}\text{C}/\text{km}$  (e.g., Henry, 1981) since 60 Ma implies that the northernmost sample has been exhumed from a depth of  $\leq 2.5$  km since  $\sim 41$  Ma, whereas the samples to the south of the Naranjo Fault Zone have been exhumed from a depth of  $\leq 3.5$  km. Therefore, the rocks exposed in the southern zone of

## North of Naranjo Fault Zone

99RS18

## South of Naranjo Fault Zone

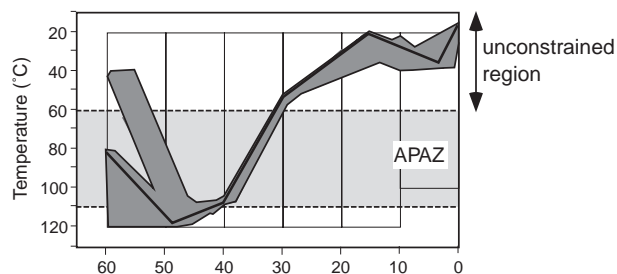
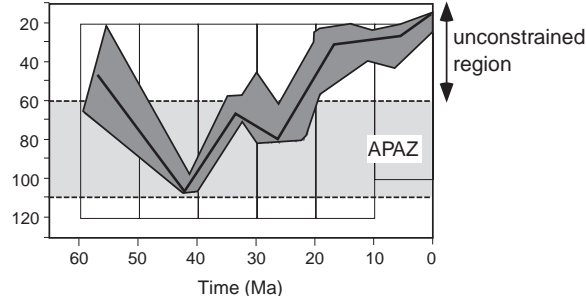
99RS2299RS24

Fig. 7. 95% confidence thermal history envelopes for samples from the Amotape Complex generated using the same principle described in Fig. 6 and an unannealed track length of 15.5  $\mu\text{m}$ . The line of best fit in each model is shown and the ZFT age of sample 99RS18 is plotted on the thermal history path. Boxes highlight the temperature–time constraints on individual inflection points within each model. APAZ: apatite partial annealing zone, ZPAZ: zircon partial annealing zone.

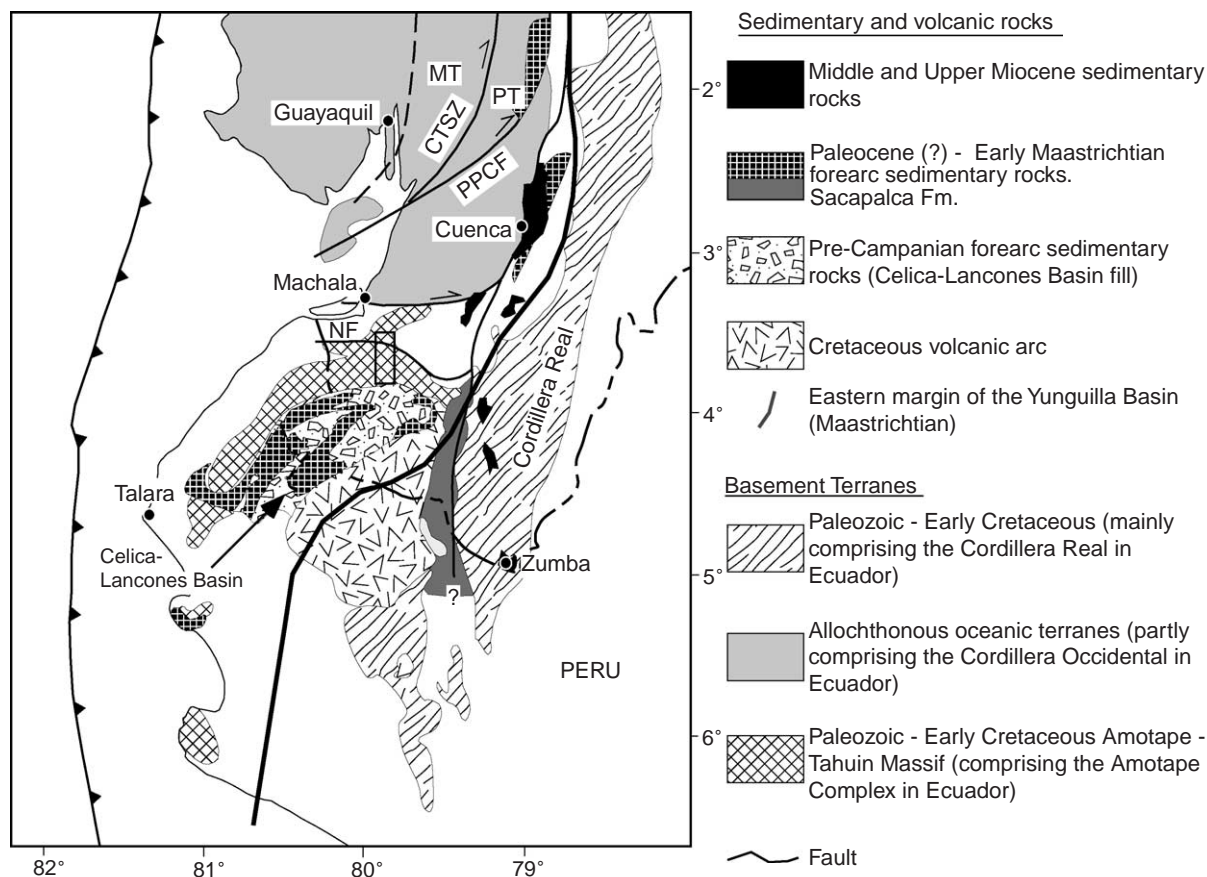


Fig. 8. Regional geology of southwestern Ecuador and northwestern Peru, showing the spatial relationship between the Amotape Complex, the Cordillera Occidental and the Yunguilla Basin. The rectangular box highlights the sampled traverse across the Amotape Complex. Faults: CTSZ: Chimbo–Toachi Shear Zone, NF: Naranjo fault, PPCF: Pujilí–Pallatanga–Calacali fault. MT: Macuchi Terrane, PT: Pallatanga Terrane. Compiled from Jaillard et al. (1999) and Hungerbühler et al. (2002).

the Amotape Complex have been uplifted relative to the northern zone since ~43 Ma, possibly by reactivation of the fault.

The most contrasting feature of the data from the Amotape Complex is the difference in the ZFT ages obtained from the northern and southern zones. ZFT and AFT ages of sample 99RS18 (northern zone) are similar, implying that the sample experienced a significant cooling event during 75(?)–65 Ma when it cooled from temperatures >220 °C to <80 °C (Fig. 7). Assuming that cooling was driven by exhumation, this equates to the exhumation of at least 4 km of crust during 75(?)–65 Ma. The older ZFT ages of samples to the south of the Naranjo Fault Zone preserve an older cooling history, implying that any

cooling during 75–65 Ma was lower than in the northern province, which may be a consequence of lower amounts of exhumation. The form of the pre-60 Ma thermal history of the southern province cannot be determined with the current data set. However, biotite  $^{40}\text{Ar}/^{39}\text{Ar}$  plateau and ZFT ages from Early Palaeozoic sedimentary rocks ( $213 \pm 1$  to  $139 \pm 10$  Ma) record post-depositional heating to temperatures >220 °C, which was probably caused by burial and metamorphism (e.g., Aspiden et al., 1995). Similarly, the significant discrepancy between the ZFT age of the Marcabeli Pluton and its crystallisation and biotite K/Ar cooling ages (Noble et al., 1997; Aspiden et al., 1995) is probably the result of exhumation subsequent to magmatic emplacement. Furthermore, the

similarity in ZFT ages from the Marcabelli Pluton and Early Paleozoic sedimentary rocks (e.g., 99RS25) suggests that most post-magmatic exhumation probably occurred at ~140 Ma, which is coincident with the postulated timing of terrane accretion in the Cordillera Real (Mourier et al., 1988; Litherland et al., 1994).

### 5.3. The significance of age populations that are older than their stratigraphic ages

Several sedimentary and volcanic rocks from the Cordillera Occidental yield multiple ZFT age populations (Fig. 5). A majority of the older populations are older than the stratigraphic age of the sample, indicating that they have not been fully reset since they last underwent lithification. Therefore, the ZFT data from these populations provide information that constrains their source terranes (e.g., Carter and Bristow, 2000). The oldest age obtained from the oceanic basement is  $123 \pm 12$  Ma (Sm/Nd) from a gabbro of the San Juan unit (Fig. 2; Mamberti et al., 1999). Furthermore, assuming that the basement Pallatanga unit is a remnant of the Caribbean Plateau, its age is probably ~100–90 Ma (Sinton et al., 1998; Spikings et al., 2001). Therefore, the older ZFT ages of 322–166 Ma, obtained from populations contained within arenites of the early Paleocene–late Eocene Angamarca group (Table 1; Fig. 5), and the distinctly older biotite  $^{40}\text{Ar}/^{39}\text{Ar}$  plateau age from detrital grains of the Campanian Mulaute unit, record relic cooling of the source rocks in the Cordillera Real, confirming contemporaneous sediment derivation from the east. Consequently, the Mulaute unit is probably not entirely a pre-accretionary sequence and is at least partly coeval with the accretion of the Pallatanga Terrane. The data cannot be used to distinguish between potential source regions for populations with ZFT ages younger than ~125 Ma.

## 6. Implications

### 6.1. Timing of terrane accretion in the Cordillera Occidental and reactivation of the Amotape Complex

Rapid cooling ( $<80$  °C/my) of the tectonic mélange (Pujilí Fm.), which formed in the suture zone between

oceanic crust of the Pallatanga Terrane and the continental margin (Hughes and Pilatasig, 2002) during 85–60 Ma was probably a result of regional exhumation that accompanied the collision (Fig. 6). Therefore, assuming that the mélange formed during the early stages of the collision, the suture can be dated at ~85 Ma and the progressive formation of the mélange via reactivation of the suture probably continued until ~60 Ma. This corroborates with previous studies, which utilised a cluster of partially (?) reset K/Ar ages at 90–50 Ma (Feininger, 1982; Herbert and Pichler, 1983; Aspdén et al., 1992) in the Cordillera Real to postulate that oceanic crust accreted against the continental margin at some time during 85–55 Ma. The collision of oceanic crust with the continental margin between 85 and 60 Ma culminated with a dramatic increase in exhumation rates in the Cordillera Real at 65–55 Ma (Spikings et al., 2000, 2001). Rapid cooling (Fig. 6) during 74–65 Ma of a sandstone block, which forms part of the mélange, pre-dates its stratigraphic age and hence reflects cooling of the source rather than the mélange. It is not clear when the sandstone block became incorporated into the mélange although heating of the block during 64–55 Ma may have been caused by burial during reactivation and growth of the mélange. The Cordillera Occidental formed part of a sub-aerial, forearc basin during the Campanian–Maastrichtian ('Yunguilla Basin' of Jaillard et al., 1999; Hughes and Pilatasig, 2002; Fig. 8) and hence the collision and prolonged reactivation of the suture during 85–60 Ma was not accompanied by the emergence of topography along the suture zone. Rocks presently exposed in the mélange have remained cooler than ~60 °C since ~32 Ma, indicating that post accretionary deformation and exhumation in the Cordillera Occidental has been localised farther west (probably along the Chimbo–Toachi Shear Zone), where the rocks preserve a younger cooling history. The thermochronological evidence for Late Cretaceous accretion of the Pallatanga Terrane in the Cordillera Occidental of Ecuador is consistent with the regional evidence described by Bourgois et al. (1990) and Kellogg and Vega (1995) for the accretion of oceanic rocks to the continental margin in the Cordillera Occidental of Colombia.

Late Eocene–Recent volcanic rocks in the Interandean Depression obscure the eastward limit of the mélange zone although it may correspond with the



Peltetec mélange exposed along the western flank of the Cordillera Real (described in Litherland et al., 1994; Fig. 1), which hosts blocks with similar lithologies to those found in the Pujilí Fm. No thermal history paths have been directly derived from the Peltetec mélange although the Cordillera Real was exhuming rapidly during 65–55 Ma (Spikings et al., 2001). Furthermore, elevated cooling and exhumation of the extensive Palenque Mélange Division, exposed north of the Naranjo Fault Zone in the Amotape Complex during 75–65 Ma (Fig. 7) were simultaneous with that in the Pujilí Fm. Therefore, while unproven, it is reasonable to postulate that the Pujilí Fm., Palenque Mélange Division, and the Peltetec mélange formed a continuous tectonised zone that formed during the collision of the Pallatanga Terrane with the continental margin at ~85 Ma. It is important to note that the Peltetec mélange and the Palenque Mélange Division may have existed prior to the collision (Mourier et al., 1988; Litherland et al., 1994; Aspden et al., 1995) and they may have simply been reactivated during the Campanian–lower Paleocene.

Regional stratigraphic and geochronological evidence in the Cordillera Occidental (BGS-CODIGEM, 1999; Hughes and Pilatasig, 2002) and increased exhumation rates in the Cordillera Real during 43–30 Ma (Spikings et al., 2001) indicate that the Macuchi Terrane accreted with the Pallatanga Terrane along the Chimbo–Toachi Shear Zone (Fig. 2) during late Eocene times. Mylonitised basaltic andesites within the Chimbo–Toachi Shear Zone have been reset by younger, late Miocene events and hence the timing of accretion cannot be directly confirmed from the data in this study. However, (i) rapid cooling of Maastriichtian sandstones (Fig. 6) in the far northern Cordillera Occidental at ~40 Ma and (ii) cooling of an early–middle Paleocene sandstone block that is exposed within the Pujilí Fm. (tectonic mélange) during ~42–32 Ma, may be a result of exhumation driven by the collision of the Macuchi Terrane.

The onset of increased cooling and exhumation rates in both provinces of the Amotape Complex at ~43–39 Ma (Fig. 7) is interpreted to result from increased compressive stress generated by the collision of the Macuchi Terrane with the SOAM margin. The fission-track data and cooling history of the Amotape Complex are remarkably similar to the southern Cordillera Real (south of 2°45' S; Spikings

et al., 2001), implying that both regions experienced a similar tectonic regime during the Cenozoic following their tectonic separation. Palaeomagnetic reconstructions of autochthonous, late Aptian sediments of the Celica–Lancones Basin (Mourier et al., 1988; Fig. 8), which were partly deposited over the Amotape Complex (Jaillard et al., 1999) suggest that the complex has undergone ~63° of clockwise rotation since ~115–110 Ma. Furthermore, ~25° of this rotation has probably occurred since the late Paleocene (Mitouard et al., 1990). Therefore, we suggest that a majority of the ~38° of clockwise rotation, that is loosely constrained to have occurred at some time between ~115 and 53 Ma, may have been simultaneous with increased exhumation rates in the Amotape Complex during ~75–65 Ma. Similarly, a majority of post late Paleocene rotation probably coincided with increased exhumation rates during ~43–29 Ma.

## 6.2. Miocene–recent cooling and the origin of the Interandean Depression

Pilger (1984) and Daly (1989) speculate, on the basis of plate convergence rates, that the Carnegie Ridge (Fig. 1) first collided with the Ecuadorian Trench at ~8 Ma. However, Spikings et al. (2001) combined the same and more recent convergence plate movement data (e.g., Pardo-Casas and Molnar, 1987; Norabuena et al., 1999) with thermal history data from the Cordillera Real and suggested the initial collision occurred at ~15 Ma, with subsequent coupling at ~9 Ma. Fault bounded blocks, which expose the Pilatón unit and the Silante unit may record cooling at ~15–13 Ma in northern Ecuador (Fig. 6) although the data from the Cordillera Occidental are sparse and cannot be used to resolve this debate.

Localised post-accretionary cooling of the Silante unit at ~9 Ma (Fig. 6) is probably a consequence of an increased exhumation rate generated by the reactivation and uplift of fault blocks, which formed small scale massifs in the Pallatanga Terrane. Imprecise AFT ages of  $7 \pm 4$  Ma (Undifferentiated Metamorphics unit) and  $9 \pm 3$  Ma (Macuchi unit) and AFT ages of  $11 \pm 2$  and  $8 \pm 2$  Ma (sedimentary cover sequences of the Pallatanga Terrane) occur over an altitude range of ~1100 m (Fig. 9). This trend suggests that a large part of the Cordillera Occidental,

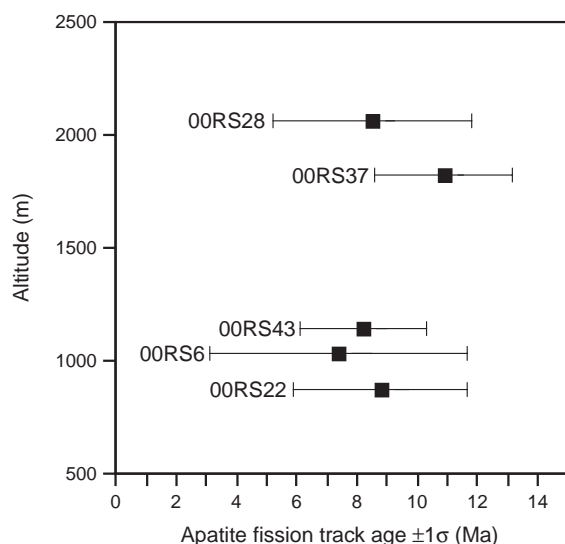


Fig. 9. Comparison between the AFT age and altitude of samples, which yield late Miocene AFT ages. The samples are from geographically disperse regions of the Cordillera Occidental and cover an altitude range of ~1100 m, indicating that the Cordillera Occidental was rapidly exhumed as a coherent block on a large scale during the late Miocene.

located to the west of the Pallatanga–Pujilí–Calacali fault, was exhumed through the apatite partial annealing zone as a coherent block during the middle–late Miocene. This corroborates the stratigraphic and sedimentological evidence from the southern Ecuadorian forearc region, which implies that the topography of the Cordillera Occidental south of  $\sim 2^{\circ}30'$  S began to form at  $\sim 9$  Ma (Steinmann et al., 1999). Furthermore, Spikings et al. (2000) recorded a sudden increase in cooling and exhumation rates ( $\sim 1.7$  km/my) in the northern Cordillera Real at  $\sim 8.5$  Ma (Fig. 6). Periods of cooling at  $\sim 9$ – $8$  Ma have also been recognised in Venezuela, Colombia, Peru, Bolivia and northern Argentina (see review in Spikings et al., 2000), which suggests that a plate-scale process may have occurred, possibly driven by increased half-spreading rates in the equatorial Atlantic at  $\sim 9$ – $8$  Ma (Brozena, 1986).

Late Miocene and younger FT ages (Fig. 2) are restricted to highly strained rocks, which form part of the Chimbo–Toachi Shear Zone. Their fission track data cannot be modelled to determine thermal history paths and hence it is not obvious how these ages relate to the thermal histories of the minerals and the deformation history of the rocks. However, the ZFT

chronostratigraphy of the intermontane Chota Basin, located in the far northern Interandean Depression (Fig. 2), suggests that the oldest sedimentary rocks are 6–5 Ma (e.g., Winkler et al., 2002; Fig. 2). These are the oldest sedimentary rocks in the Interandean Depression and probably approximate the timing of inception of the Chota Basin. Therefore, there may have been a single topographic chain north of  $\sim 2^{\circ}30'$  S in Ecuador prior to  $\sim 6$  Ma. Late Miocene cooling (from temperatures of 90–80 °C) and exhumation rates of  $\sim 0.7$  km/my during 5–0 Ma are recorded in the northernmost Cordillera Real at  $\sim 0^{\circ}30'$  N (Spikings et al., 2000; Fig. 6). Collectively, this evidence suggests that late Miocene and younger fission track ages from the Chimbo–Toachi Shear Zone may record cooling that followed a period of shearing and accompanied exhumation at  $\sim 6$ – $5$  Ma. Dextral strike-slip displacement of the allochthonous oceanic terranes towards the north–northeast since  $\sim 6$  Ma produced a complex transcurrent system that included the La Sofia (e.g., Ego et al., 1996), Pallatanga (e.g., Winter et al., 1993) and Chimbo–Toachi faults, and uplifted fault blocks comprising the northern cordillera (Fig. 1). The same system generated the Chota Basin and later the Pliocene–Pleistocene Latacunga, Quito and Guayllabamba basins (Figs. 1 and 2; Lavenu et al., 1995; Ego and Sebrier, 1996; Winkler et al., 2002), which collectively form parts of the Interandean Depression. The Interandean region south of  $\sim 2^{\circ}30'$  S hosts middle–upper Miocene sedimentary basins (Fig. 8), which preserve an older continental, inter-montane sedimentary sequence with ages between  $\sim 9$  and 7.5 Ma (Steinmann et al., 1999; Hungerbühler et al., 2002). This region has been in a state of uplift since  $\sim 9$  Ma (Steinmann et al., 1999), which contrasts markedly with the Interandean Depression, which is characterised by differential subsidence relative to the bordering cordilleras since 6–5 Ma. The southern region may be isolated from the transcurrent system, which formed the Interandean Depression, by reactivation of the southern Pallatanga–Pujilí–Calacali fault.

## 7. Conclusions

1. The formation and subsequent reactivation of the tectonic mélange, exposed at the eastern margin of

the Cordillera Occidental at 85–60 Ma, probably dates the timing of collision of the Pallatanga Terrane with the continental margin and subsequent reactivation of the suture, respectively. In addition, the reactivation and exhumation of the Palenque Mélange Division of the Amotape Complex during 75–65 Ma, suggests that the collision resulted in a tectonised zone that extended as far south as  $\sim 5^{\circ}\text{S}$ . The Late Cretaceous Pallatanga collision event may also be responsible for decoupling of the Amotape Complex from the Cordillera Real via a clockwise rotation of  $38^{\circ}$ . The Pujilí Fm., Palenque Mélange Division and the Peltetec mélange may constitute a single, continuous tectonised zone that formed during the collision of the Pallatanga Terrane with the continental margin at  $\sim 85$  Ma and subsequent reactivation until  $\sim 60$  Ma. Previous models, which propose that the Peltetec mélange and other rocks, which comprise the Cordillera Real, collided and deformed at 140 Ma may be inaccurate.

2. The timing of accretion of the Macuchi Terrane with the Pallatanga Terrane cannot be directly determined from the data obtained here as a majority of rocks that were deformed by the formation of the Chimbo–Toachi Shear Zone have been reset by younger tectonic events. However, rapid exhumation of local fault blocks within the Cordillera Occidental at  $\sim 40$  Ma and reactivation of parts of the Pallatanga–Pujilí–Calacali fault during 42–32 Ma are entirely consistent with previous interpretations (Hughes and Pilatasig, 2002) of the accretion of the Macuchi Terrane in the late Eocene. The onset of rapid exhumation at 43–39 Ma in the Amotape Complex probably coincided with  $25^{\circ}$  of clockwise rotation as a result of the accretion of the Macuchi Terrane, which confirms previous estimates of the timing of collision.
3. Distinct periods of rapid exhumation of local fault blocks in the Cordillera Occidental occurred at  $\sim 13$  and  $\sim 9$  Ma. Cooling at  $\sim 13$  Ma is probably the result of the collision of the Carnegie Ridge (e.g., Spikings et al., 2001). With the exception of the Pallatanga–Pujilí–Calacali fault, reactivation at 9 Ma was geographically widespread and exhumed the entire length of the Cordillera in both the Pallatanga and Macuchi Terranes, implying a large

scale change in the tectonic regime, probably as a result of dextral displacement of coastal Ecuador driven by coupling of the upper plate with the subducting Carnegie Ridge. The same events are not recognised in the Amotape Complex suggesting that it was isolated from the changing stress field, probably via reactivation of either the Pallatanga–Pujilí–Calacali fault or the Chimbo–Toachi Shear Zone.

4. Late Miocene–Pliocene reactivation of the Chimbo–Toachi Shear Zone coincides with the earliest deposition of sedimentary rocks in the Interandean Depression and rapid exhumation in the northern Cordillera Real. Therefore, the Chimbo–Toachi Shear Zone probably formed part of a complex transcurrent system during the late Miocene–Pliocene that was responsible for opening of the Interandean Depression at  $\sim 6$ –5 Ma within a transcurrent setting.
5. Detrital ZFT age populations from arrenites of the early Paleocene–late Eocene Angamarca group show that it was at least partly derived from exhumation of the Cordillera Real. Several ZFT age populations from the Angamarca group yield ages between 322 and 166 Ma, which are older than the basement in the Pallatanga and Macuchi Terranes. However, the ZFT ages are similar to a range of ZFT ages obtained from several fault-bounded blocks in the Cordillera Real, implying that these blocks were contributing sediment to the Angamarca group. Similarly, Triassic detrital  $^{40}\text{Ar}/^{39}\text{Ar}$  ages from the Campanian Mulaute group suggest it is probably not entirely a pre-accretionary sequence and is at least partly coeval with the accretion of the Pallatanga Terrane.

### Acknowledgements

The authors would like to express their thanks to Bernado Beate (EPN-Quito), John Aspden (BGS), Bill McCourt (BGS) and Warren Pratt for several interesting discussions regarding accretionary events in Ecuador. Field sampling benefited from the assistance and knowledge of Diego Villagomez (EPN-Quito). Funding for the project was provided by the Swiss National Science Foundation, project number 20-56794-99.

## Appendix A. Sample preparation and analysis

Mineral separation and analytical procedures for  $^{40}\text{Ar}/^{39}\text{Ar}$  and fission track analysis followed those outlined by Spikings et al. (2001). Hornblende, white mica and biotite separates were sealed in quartz vials and irradiated in the MTA KFKI reactor (Debrecen, Hungary) for 16 h. Correction factors for interfering isotopes have been calculated from 10 analyses of two Ca-glass samples and 22 analyses of two pure K-glass samples, and are:  $^{36}\text{Ar}/^{37}\text{Ar}_{(\text{Ca})}=2.603\text{E}-4\pm 2.373\text{E}-9$ ,  $^{39}\text{Ar}/^{37}\text{Ar}_{(\text{Ca})}=6.501\text{E}-4\pm 7.433\text{E}-9$  and  $^{40}\text{Ar}/^{39}\text{Ar}_{(\text{K})}=1.547\text{E}-2\pm 7.455\text{E}-7$ . Apatites and zircons were irradiated at the Australian HIFAR reactor with average neutron fluences of  $1\times 10^{16}$  and  $1\times 10^{15}$  n/cm<sup>2</sup>, respectively. Neutron fluences were monitored using DRA1 sanidine ( $^{40}\text{Ar}/^{39}\text{Ar}$  analysis; Wijbrans et al., 1995), CN1 standard glass (ZFT analysis) and CN5 standard glass (AFT analysis).

Gas was extracted from the ferromagnesian phases at the Institute for Geology and Paleontology at the University Salzburg in a step-wise manner using a Merchantek™ PC controlled, defocused, 25W CO<sub>2</sub>-IR laser, cleaned using hot and cold Zr-Al SAES getters and analysed using a VG-Isotech™ VG3600 mass spectrometer. Measurements were recorded by an axial electron multiplier in static mode.  $^{36}\text{Ar}$ ,  $^{37}\text{Ar}$ ,  $^{38}\text{Ar}$ ,  $^{39}\text{Ar}$  and  $^{40}\text{Ar}$  isotope intensities were corrected for system blanks, background, post-irradiation decay of  $^{37}\text{Ar}$  and interfering isotopes.  $^{40}\text{Ar}/^{39}\text{Ar}$  ages and errors were calculated following the suggestions of McDougall and Harrison (1999) using the decay constants of Steiger and Jäger (1977). The identification of and calculation of plateau ages were performed using ISOPLLOT/EX (Ludwig, 2001).

Fossil fission tracks were revealed in zircons by etching in the eutectic mixture of NaOH/KOH at 210 °C for periods between 5 and 60 h and in apatite by etching in 5 N HNO<sub>3(aq)</sub> at 21 °C for 20 s. When individual ZFT age populations were expected to be present in any individual sample the sample was split into three aliquots and each aliquot was etched separately. Each zircon aliquot was considered to be fully etched when fission tracks in each individual population (identified by grain colour and shape) were clearly visible parallel to the crystal *c*-axis in euhedral grains. Induced tracks were revealed in muscovite external detectors by etching in 40% HF<sub>(aq)</sub> at 21 °C

for 45 min. Fission tracks were counted at a magnification of 1250× (apatite) and 1600× (zircon, dry objective) using computer controlled Zeiss microscopes and the Kinetec™ stage. Only those apatites and zircons mounted in the plane of the crystallographic *c*-axis were counted. Lengths of horizontal confined tracks were measured in apatite grains lying in the plane of the *c*-axis using a drawing tube and digitising tablet. A majority of apatites analysed in this study have uranium concentrations <10 ppm and hence very few samples yielded useful track-length information (Table 1). Analytical procedures followed the external detector method described by Gleadow (1981). Ages were calculated using the zeta calibration method (Hurford and Green, 1983) and errors were calculated according to conventional methods (Green, 1981) and are reported at the 1σ level. All samples were counted by R. Spikings with zeta calibration factors of  $134.7\pm 3.1$  (zircon, CN1 glass) and  $387\pm 17$  (apatite, CN5 glass).

## References

- Arculus, R.J., Lapierre, H., Jaillard, E., 1999. Geochemical window into subduction and accretion processes: Rasapas metamorphic complex, Ecuador. *J. Geol.* 27, 547–550.
- Aspden, J.A., Litherland, M., 1992. The geology and Mesozoic collisional history of the Cordillera Real, Ecuador. *Tectonophysics* 205, 187–204.
- Aspden, J.A., Harrison, S.H., Rundle, C.C., 1992. New geochronological control for the tectono-magmatic evolution of the metamorphic basement, Cordillera Real and El Oro Province of Ecuador. *J. South Am. Earth Sci.* 6, 77–96.
- Aspden, J.A., Bonilla, W., Duque, P., 1995. The El Oro metamorphic complex, Ecuador: geology and economic mineral deposits. *Overseas Geology and Mineral Resources*, vol. 67. British Geological Survey. 63 pp.
- Bourgeois, J., Eguez, A., Butterlin, J., De Wever, P., 1990. Evolution géodynamique de la Cordillere Occidentale des Andes d'Equateur: la découverte de la formation Eocene d'Apagua. *C. R. Acad. Sci., Paris* 311, 173–180.
- British Geological Survey–CODIGEM, 1997a. Mapa geológico de la Cordillera Occidental del Ecuador entre 2°S–3°S. Dirección Nacional de Geología, Quito, Ecuador, scale 1:200 000, 1 sheet.
- British Geological Survey–CODIGEM, 1997b. Mapa geológico de la Cordillera Occidental del Ecuador entre 1°S–2°S. Dirección Nacional de Geología, Quito, Ecuador, scale 1:200 000, 1 sheet.
- British Geological Survey–CODIGEM, 1999. Mapa geológico de la Cordillera Occidental del Ecuador entre 0°–1°S. Dirección Nacional de Geología, Quito, Ecuador, scale 1:200 000, 1 sheet.
- British Geological Survey–CODIGEM, 2000. Mapa geológico de la Cordillera Occidental del Ecuador entre 0°–1°N. Dirección



- Nacional de Geología, Quito, Ecuador, scale 1:200 000, 1 sheet.
- Brozena, J.M., 1986. Temporal and spatial variability of seafloor spreading processes in northern South Atlantic. *J. Geophys. Res.* 1, 497–510.
- Carlson, W.D., Donelick, R.A., Ketcham, R.A., 1999. Variability of apatite fission-track annealing kinetics: I. Experimental results. *Am. Mineral.* 84, 1213–1223.
- Carter, A., Bristow, C.S., 2000. Detrital zircon geochronology: enhancing the quality of sedimentary source information through improved methodology and combined U–Pb and fission-track techniques. *Basin Res.* 12, 47–57.
- Daly, M.C., 1989. Correlations between Nazca/Farallon plate kinematics and forearc basin evolution in Ecuador. *Tectonics* 8, 769–790.
- Dodson, M.H., 1973. Closure temperature in cooling geochronological and petrological systems. *Contrib. Mineral. Petrol.* 40, 259–274.
- Ego, F., Sebrier, M., 1996. The Ecuadorian Interandean Depression: a major and complex restraining bend and compressive graben since late Miocene time. *Ann. Tecton.*, 31–59.
- Ego, F., Sebrier, M., Lavenue, A., Yepes, H., Eques, A., 1996. Quaternary state of stress in the northern Andes and the restraining bend model for the Ecuadorian Andes. *Tectonophysics* 259, 101–116.
- Faucher, B., Vernet, R., Bizon, G., Bizon, J.J., Grekoff, N., Lys, M., Sigal, J., 1971. Sedimentary formations in Ecuador. A stratigraphic and micropaleontological survey. *Bur. Étud. Ind. Coop. Inst. Fr. Pét.* 3 (220 pp.).
- Feininger, T., 1982. The metamorphic “basement” of Ecuador. *Geol. Soc. Amer. Bull.* 93, 87–92.
- Feininger, T., 1987. Allochthonous terranes in the Andes of Ecuador and northwestern Peru. *Can. J. Earth Sci.* 94, 266–278.
- Feininger, T., Bristow, C.R., 1980. Cretaceous and Paleogene history of coastal Ecuador. *Geol. Rundsch.* 69, 849–874.
- Feininger, T., Seguin, M.K., 1983. Simple Bouguer gravity anomaly field and the inferred crustal structure of continental Ecuador. *J. Geol.* 11, 40–44.
- Feininger, T., Silberman, M.L., 1982. K–Ar geochronology of basement rocks on the northern flank of the Huancabamba Deflection, Ecuador. U.S. Geological Survey Open-File Report 83-206 (paper copy), 21 pp.
- Galbraith, R.F., Green, P.F., 1990. Estimating the component ages in a finite mixture. *Nucl. Tracks Radiat. Meas.* 17, 197–206.
- Gallagher, K., 1995. Evolving thermal histories from fission-track data. *Earth Planet. Sci. Lett.* 36, 421–435.
- Gleadow, A.J.W., 1981. Fission-track dating methods: what are the real alternatives? *Nucl. Tracks Radiat. Meas.* 5, 3–14.
- Gleadow, A.J.W., Duddy, I.R., Green, P.F., Heggarty, K.A., 1986. Fission track lengths in the apatite annealing zone and the interpretation of mixed ages. *Earth Planet. Sci. Lett.* 78, 245–254.
- Green, P.F., 1981. A new look at statistics in fission-track dating. *Nucl. Tracks Radiat. Meas.* 5, 77–86.
- Green, P.F., Duddy, I.R., Gleadow, A.J.W., Tingate, P.R., Laslett, G.M., 1986. Thermal annealing of fission tracks in apatite: I. A qualitative description. *Chem. Geol.* 59, 237–253.
- Henry, S., 1981. Terrestrial Heat Flow Overlying the Andean Subduction Zone. PhD thesis, Michigan, University of Michigan, 184 pp.
- Herbert, H.J., Pichler, H., 1983. K–Ar ages of rocks from the Eastern Cordillera of Ecuador. *Z. Dtsch. Geol. Ges.* 134, 483–493.
- Hughes, R.A., Pilatasig, L.F., 2002. Cretaceous and Tertiary terrane accretion in the Cordillera Occidental of the Ecuadorian Andes. *Tectonophysics* 345, 29–48.
- Hungerbühler, D., Steinmann, M., Winkler, W., Seward, D., Egüez, A., Peterson, D.E., Helg, U., Hammer, C., 2002. Neogene stratigraphy and Andean geodynamics of southern Ecuador. *Earth-Sci. Rev.* 57, 75–124.
- Hurford, A.J., Green, P.F., 1983. The zeta calibration of fission-track dating. *Isot. Geosci.* 1, 285–317.
- Jaillard, E., Laubacher, G., Bengston, P., Dhondt, A.V., Butlo, L.G., 1999. Stratigraphy and evolution of the Cretaceous forearc Celica–Lancones basin of southwestern Ecuador. *J. South Am. Earth Sci.* 12, 51–68.
- Kellogg, J.N., Vega, V., 1995. Tectonic development of Panama, Costa Rica, and the Colombian Andes: constraints from global positioning system geodetic studies and gravity. In: Mann, P. (Ed.), *Geologic and Tectonic Development of the Caribbean Plate Boundary in Southern Central America*, Spec. Pap. Geol. Soc. Am., vol. 295, pp. 75–90.
- Laslett, G.M., Green, P.F., Duddy, I.R., Gleadow, A.J.W., 1987. Thermal annealing of fission tracks in apatite: 2. A quantitative analysis. *Chem. Geol.* 65, 1–15.
- Lavenue, A., Winter, T., Dávila, F.A., 1995. Pliocene–Quaternary compressional basin in the Interandean Depression, Central Ecuador. *Geophys. J. Int.* 121, 279–300.
- Lebrat, M., Megard, F., Dupuy, C., Dostal, J., 1987. Geochemistry and tectonic setting of pre-collisional Cretaceous and Paleogene volcanic rocks of Ecuador. *Geol. Soc. Amer. Bull.* 99, 469–578.
- Litherland, M., Aspdén, J., Jemielita, R.A., 1994. The metamorphic belts of Ecuador. *Overseas Mem.-Br. Geol. Surv.* 11 (147 pp.).
- Ludwig, K.R., 2001. *Isoplot/Ex-A geochronological toolkit for Microsoft Excel*. Berkeley Geochronological Center Special Publication 1a.
- Mamberti, M., Bosch, D., Lapierre, H., Hernandez, J., Jaillard, E., Polve, M., 1999. Petrology and geochemistry of Mg-rich basalts from Western Ecuador: remnants of the Late Cretaceous Caribbean Plateau. *Proceedings, International Symposium on Andean Geodynamics*, 4th, Göttingen, Germany, pp. 832–835.
- McCourt, W.J., Aspdén, J.A., Brook, M., 1984. New geological and geochronological data from the Colombian Andes: continental growth by multiple accretion. *J. Geol. Soc. (Lond.)* 141, 831–845.
- McDougall, I., Harrison, T.M., 1999. *Geochronology and Thermochronology by the  $^{40}\text{Ar}/^{39}\text{Ar}$  Method*. Oxford Univ. Press, New York. 269 pp.
- Mitouard, P., Kissel, C., Laj, C., 1990. Post-Oligocene rotations in southern Ecuador and northern Peru and the formation of the Huancabamba Deflection in the Andean Cordillera. *Earth Planet. Sci. Lett.* 98, 329–339.
- Mourier, T., Laj, C., Megard, F., Roperch, P., Mitouard, P., Farfan Medrano, A., 1988. An accreted continental terrane in north-western Peru. *Earth Planet. Sci. Lett.* 88, 182–192.



- Noble, S.R., Aspden, J.A., Jamielita, R., 1997. Northern Andean crustal evolution: new U–Pb geochronological constraints from Ecuador. *Geol. Soc. Amer. Bull.* 109, 789–798.
- Norabuena, E.O., Dixon, T.H., Stein, S., Harrison, C.G.A., 1999. Decelerating Nazca–South America and Nazca–Pacific plate motions. *Geophys. Res. Lett.* 26, 3405–3408.
- Pardo-Casas, F., Molnar, P., 1987. Relative motion of the Nazca (Farallon) and South America plate since Late Cretaceous time. *Tectonics* 6, 233–248.
- Pilger, R.H., 1984. Cenozoic plate kinematics subduction and magmatism: South American Andes. *J. Geol. Soc. (Lond.)* 141, 793–802.
- Sinton, C.W., Duncan, R.A., Storey, M., Lewis, J., Estrada, J.J., 1998. An oceanic flood basalt province within the Caribbean plate. *Earth Planet. Sci. Lett.* 155, 221–235.
- Spikings, R.A., Seward, D., Winkler, W., Ruiz, G.M., 2000. Low-temperature thermochronology of the northern Cordillera Real, Ecuador: tectonic insights from zircon and apatite fission track analysis. *Tectonics* 19, 649–668.
- Spikings, R.A., Winkler, W., Seward, D., Handler, R., 2001. Along-strike variations in the thermal and tectonic response of the continental Ecuadorian Andes to the collision with heterogeneous oceanic crust. *Earth Planet. Sci. Lett.* 186, 57–73.
- Steiger, R.H., Jäger, E., 1977. Subcommittee on geochronology: convention on the use of decay constants in geo- and cosmochronology. *Earth Planet. Sci. Lett.* 36, 359–362.
- Steinmann, M., 1997. Fission track age determinations on zircons, Ecuador. British Geological Survey–CODIGEM. Dirección Nacional de Geología, Quito, Ecuador. 59 pp.
- Steinmann, M., Hungerbühler, D., Seward, D., Winkler, W., 1999. Neogene tectonic evolution and exhumation of the southern Ecuadorian Andes: a combined stratigraphy and fission-track approach. *Tectonophysics* 307, 255–276.
- Tagami, T., Galbraith, R.F., Yamada, R., Laslett, G.M., 1998. Revised annealing kinetics of fission tracks in zircon and geological implications. In: Van den Haute, P., de Corte, F. (Eds.), *Advances in Fission-Track Geochronology*. Kluwer Academic Publishers, Dordrecht, pp. 99–112.
- Vrolijk, P., Donelick, R.A., Queng, J., Cloos, M., 1992. Testing models of fission track annealing in apatite in a simple thermal setting. *Proceedings of the Ocean Drilling Program, Scientific Results, Site 800, Leg 129*, pp. 169–176.
- Wijbrans, J.R., Pringle, M.S., Koopers, A.A.P., Schveers, R., 1995. Argon geochronology of small samples using the Vulkaan argon laserprobe. *Proceedings of the Koninklijke Nederlandse Akademie van Wetenschappen* vol. 98, pp. 185–218.
- Wilkinson, I.P., 1998a. Foraminifera from a suite of Late Cretaceous and Palaeogene samples from the Cordillera Occidental Ecuador. British Geological Survey Technical Report WH/98/56R (paper copy), 5 pp.
- Wilkinson, I.P., 1998b. Calcareous Microfauna from a suite of samples from the Cordillera Occidental, Ecuador. British Geological Survey Technical Report WH/98/163R (paper copy), 6 pp.
- Winkler, W., Spikings, R., Villagomez, D., Eguez, A., Abegglen, P., Tobler, S., 2002. The Chota Basin and its significance for the formation of the Interandean Depression in Ecuador. *Proceedings of the 5th International Symposium on Andean Geodynamics*, Toulouse, France, pp. 705–708.
- Winter, T., Avouac, J.-P., Lavenue, A., 1993. Late Quaternary kinematics of the Pallatanga strike-slip fault (Central Ecuador) from topographic measurements of displaced morphological features. *J. Int.* 115, 905–920.